AN INVESTIGATION OF THE MICROSTRUCTURAL AND MECHANICAL PROPERTIES OF TRI-CALCIUM PHOSPHATES DOPED WITH ALUMINUM AND FLUORIDE IONS

A THESIS SUBMITTED TO
THE GRADUATE SCHOOL OF NATURAL AND APPLIED SCIENCES
OF
MIDDLE EAST TECHNICAL UNIVERSITY

BY

AYDIN TAHMASEBIFAR

IN PARTIAL FULLFILLMENT OF THE REQUIREMENTS
FOR
THE DEGREE OF MASTER OF SCIENCE
IN
ENGINEERING SCIENCES

AUGUST 2011

Approval of Thesis

AN INVESTIGATION OF THE MICROSTRUCTURAL AND MECHANICAL PROPERTIES OF TRI-CALCIUM PHOSPHATES DOPED WITH ALUMINUM AND FLUORIDE IONS

submitted by **AYDIN TAHMASEBIFAR** in partial fulfillment of the requirements for the degree of **Master of Science in Engineering Sciences Department, Middle East Technical University** by,

Prof. Dr. Canan Özgen _____
Dean, Graduate School of **Natural and Applied Sciences**

Prof. Dr. Turgut Tokdemir _____
Head of Department, **Engineering Sciences**

Assoc. Prof. Dr. Zafer Evis
Supervisor, **Engineering Sciences Dept., METU** _____

Examining Committee Members

Prof. Dr. Turgut Tokdemir _____
Department of Engineering Sciences, METU

Prof. Dr. Polat Saka _____
Department of Civil Engineering, Bahrain Univeraity

Assoc. Prof. Dr. Zafer Evis
Department of Engineering Sciences**,** METU _____

Assoc. Prof. Dr. Aysen Tezcaner _____
Department of Engineering Sciences, METU

Assist. Prof. Dr. Tolga Yilmaz
Department of Engineering Sciences , METU _____

24.08.2011

I hereby declare that all information in this document has been obtained and presented in accordance with academic rules and ethical conduct. I also declare that, as required by these rules and conduct, I have fully cited and referenced all material and results that are not original to this document.

Name, Last name: Aydin Tahmasebifar
Signature:

ABSTRACT

AN INVESTIGATION OF THE MICROSTRUCTURAL AND MECHANICAL PROPERTIES OF TRI-CALCIUM PHOSPHATES DOPED WITH ALUMINUM AND FLUORIDE IONS

Tahmasebifar, Aydin
M. Sc., Department of Engineering Sciences

Supervisor: Assoc. Prof. Dr. Zafer Evis

August; 88 Pages

The aim of this study was to investigate the microstructure and mechanical properties of pure tricalcium phosphate (TCP) and tricalcium phosphates doped with aluminum (Al^{3+}) and fluoride (F^-) ions at different compositions. TCP was synthesized via precipitation method and sintered at 1100°C for 1 and 5 h. It was observed that density and relative density of the sintered materials were decreased by extending the sintering time. Increased densities were achieved upon Al^{3+} and/or F^- doping. For structural analysis, XRD, SEM and FTIR spectroscopy examinations were performed. Second phases were observed in XRD studies upon doping. Due to Al^{3+} and F^- substitution, hydroxyapatite (HA) phase was detected besides β-TCP, resulting in the formation of HA/β-TCP biphasic composites with different compositions. SEM results revealed that addition of doping ions resulted in smaller grains. In FTIR analysis, in addition to the characteristic bands of TCP, novel bands indicating the substitution of F^- ions were observed in F^- ion doped samples. In general, the micro hardness test revealed that Al^{3+} ions in large amounts had negative effects on the mechanical properties of the samples, while substitution of the F^- ions had a positive effect on their mechanical properties.

Keywords: Tricalcium phosphate, Aluminum, Fluoride, Sintering, Mechanical properties.

ÖZ

ALÜMİNYUM VE FLOR İLAVE EDİLMİŞ ÜÇ-KALSİYUM FOSFATLARIN MİKROYAPISININ VE MEKANİK ÖZELLİKLERİNİN ARAŞTIRILMASI

Tahmasebifar, Aydin
Yüksek Lisans, Mühendislik Bilimleri Bölümü

Tez Yöneticisi: Doç. Dr. Zafer Evis

Ağustos; 88 Sayfa

Bu çalışmanın amacı saf üç-kalsiyum fosfatın (TCP) ve farklı kompozisyonlarda alüminyum (Al^{3+}) ve florür (F^-) iyonları ilave edilmiş üç-kalsiyum fosfatın mikroyapısının ve mekanik özelliklerinin araştırılmasıdır. TCP, çöktürme metoduyla üretilmiş ve 1100°C'de 1 ve 5 saat sinterlenmiştir. Sinterleme zamanının uzatılması ile yoğunluk ve göreceli yoğunluğun azalması gözlemlenmiştir. Al^{3+} ve/veya F^- ilave edilmesi sayesinde özkütlenin artması sağlanmıştır. Yapısal analizler için, XRD, SEM and FTIR spektroskopi incelemeleri yapılmıştır. İyon ilavesi ile ikincil fazların oluşumu XRD çalışmalarında gözlemlenmiştir. Al^{3+} and F^- iyonlarının ilavesi ile, β-TCP yanında hidroksiapatit (HA) fazı da tespit edilmiş, bu durum farklı kompozisyonlarda bifazik HA/β-TCP kompozitleri oluşumuyla sonuçlanmıştır. SEM sonuçları, iyonların eklenmesiyle daha küçük tanelerin oluştuğunu göstermiştir. FTIR analizinde, karakteristik TCP bantlarına ek olarak, F^- iyonuyla ilave edilmiş örneklerde F^- iyonlarının yer değiştirdiğini gösteren yeni bantlar gözlemlenmiştir. Genel olarak, mikrosertlik testi göstermiştir ki yüksek miktarlardaki Al^{3+} iyonlarının örneklerin mekanik özellikleri üstünde negatif etkileri varken, F^- iyonlarının ilave edilmesi örneklerin mekanik özellikleri üstünde pozitif etki oluşturmuştur.

Anahtar Kelimeler: Üç-kalsiyum fosfat, Alüminyum, Flor, Sinterleme, Mekanik Özellikler.

ACKNOWLEDGMENTS

I would like to express my special thanks to my advisor Assoc. Prof. Dr. Zafer Evis for his enthusiastic guidance and patience throughout this study. I am also so grateful to my advisor for encouraging me in this fascinating field and for letting me benefit from his profound mind and knowledge.

I would like to express my gratitude to my advisor Assoc. Prof. Dr. Zafer Evis, Assoc. Prof. Dr. Ayşen Tezcaner and Assist. Prof. Dr. Dilek Keskin for their generosities to let me work in their Biomaterials laboratory. I owe my thanks to my lab friend Sıdıka Mine Toker for her guidance during my experiments. I also would like to thank my other dear lab friends; Ömer Akturk, İdil Uysal, Yiğit Öcal, Mert Baki, Özlem Aydın, Aslı Deniz, Ayşegül Kavas and Özge Erdemli for their support, friendship and the lovely environment they created in our lab.

I would like to express my special thanks to my dearest friends Semih Erhan, Ra'ana Mousavi, Aslan Eslami Taheri, Adnan Mousavi, Yousef Zamanifard, Alireza Mazloumi and Sina Mojtahedi for their precious friendship. With their presence, the joy they bring into my life and their constant support, they mean more than friends to me.

I would like to give my greatest thanks to my parents Aziz Tahmasebifar and Farideh Tabestani for the values they taught and the endless support they provided through my entire life. Their respect and belief in what I do is precious for me.

Finally, I would like to express my very special thanks and gratitude to my brother, friend and mentor Dr. Arif Tahmasebifar (Aziz). Also my sisters Dr. Vida, Sheida and Leila Tahmasebifar. Their presence, their confidence in me, their ideas and constant support have always given me inspiration and the strength I needed at every stage of my life, as in this study.

TABLE OF CONTENTS

LIST OF TABLES

TABLES

LIST OF FIGURES

FIGURES

CHAPTER 1

1. INTRODUCTION

1.1 Apatite

The name "apatite" describes a family of compounds having similar structure (hexagonal system, space group, $P6_3/m$) to each other with the general chemical formula of $X_{10}(YO_4)_6Z_2$. Because the apatite structure is very tolerant to substitutions, various ions could be substitute into apatite [1,2]. These substituents are summarized in Table 1.1.

Table 1.1: Various ionic substitutions to apatites with a chemical formula of $X_{10}(YO_4)_6Z_2$.

X^{2+}	YO_4^{3-}	Z^-
Ca^{2+}, Ba^{2+}, Sr^{2+}, Pb^{2+}, Cd^{2+}, Mg^{2+}	PO_4^{3-}, AsO_4^{3-}, VO_4^{3-}, SiO_4^{4-}, CO_3^{2-}	F^-, OH^-, Cl^-, CO_3^{2-}

Apatite is the main inorganic constituent of hard tissues in human and animals [2]. Carbonate containing HA-like salt forms the minerals of bones and teeth. Biological apatites have nonstochiometric structures with vacant lattice sites, which considerably complicate their crystal structure. Some lattice substitutions can result in the lowering of the symmetry and/or a slight distortion from the hexagonal structure [1].

Biological apatites are poorly crystalline, which might be due to the presence of carbonate ions. Because they are known to have an essential influence on the growth of apatite crystals in solution; resulting in smaller crystals or even amorphous products [2]. Mg^{2+} ions have also the similar effect on the growth of

apatite crystals [2]. The typical composition of the inorganic components and Ca/P ratios of bone, enamel and dentin are shown in Table 1.2.

Table 1.2: Composition of the inorganic components by weight % of bone, enamel and dentin [3,4].

Component	**Enamel**	**Dentin**	**Bone (Cortical)**
Ca	37.6	40.3	36.6
P	18.3	18.6	17.1
CO_3^{2-}	3.0	4.8	4.8
Na	0.7	0.1	1.0
K	0.05	0.07	0.07
Mg	0.2	1.1	0.6
Sr	0.03	0.04	0.05
Cl	0.4	0.27	0.1
F	0.01	0.07	0.1
Ca/P molar	1.59	1.67	1.65

These values above show alterations from sample to sample; depending on the part of the tissue, species, maturation process, aging and disease [2]. From Table 1.2, it can be generally concluded that;

- The CO_3^{2-} contents of dentin and bone are similar but higher than that of the enamel
- The Mg amount of bone and dentin are higher than that of enamel and it is twice as much in the dentin compared to the bone.

- Ca/P ratio of enamel is significantly lower than the stoichiometric Ca/P ratio of 1.67 [2].

It is reported that as a result of the PO_4^{3-} replaced by CO_3^{2-} in human enamel, the Ca/P ratio is quite different than that of pure HA [5,6]. Among the calcium phosphates and apatites, HA has attracted a great deal of attention owing to its similarity to mineral part of bone.

1.2 Calcium Phosphates

Calcium phosphates (CaP) are classified as resorbable materials which dissolve under physiological conditions and can be readily assimilated by the human body [7,8]. For example, due to the resorbable nature of CaPs, with the general exception of HA, they are proposed as potential bone defect fillers [8].

1.2.1 Monocalcium Phosphates (Monohydrate and Anhydrous)

According to the CaO-P_2O_5-H_2O phase diagram, monocalcium phosphates appear in two types: the monohydrate (MCPM) with the chemical formula of $Ca(H_2PO_4)\cdot H_2O$ and the anhydrous (MCPA) with the formula of $Ca(H_2PO_4)_2$ which occurs in soluble region of the phase diagram and in acid. MCPM occurs with acidulation of rock phosphate in H_2SO_4, H_3PO_4 or HNO_3 while MCPA is made in a concentrated H_3PO_4 at high temperatures [9,10]. In Figure 1.1, illustration of the phase diagram of CaO-P_2O_5-H_2O is presented [11].

MCPMs structure is triclinic with a space group of P_1 and unit cell parameters are a=5.6261 Å, b=11.889 Å, c= 6.473 Å, α= 98.633^o, β= 118.262^o and γ= 83.344^o at 25^{o}C. The structure of MCPA is also triclinic with a space group of P_1 and unit cell parameters are a=7.5577 Å, b= 8.2531 Å, c= 5.5504 Å, α= 109.86^o, β= 93.68^o and γ= 109.15^o at 25^{o}C [11].

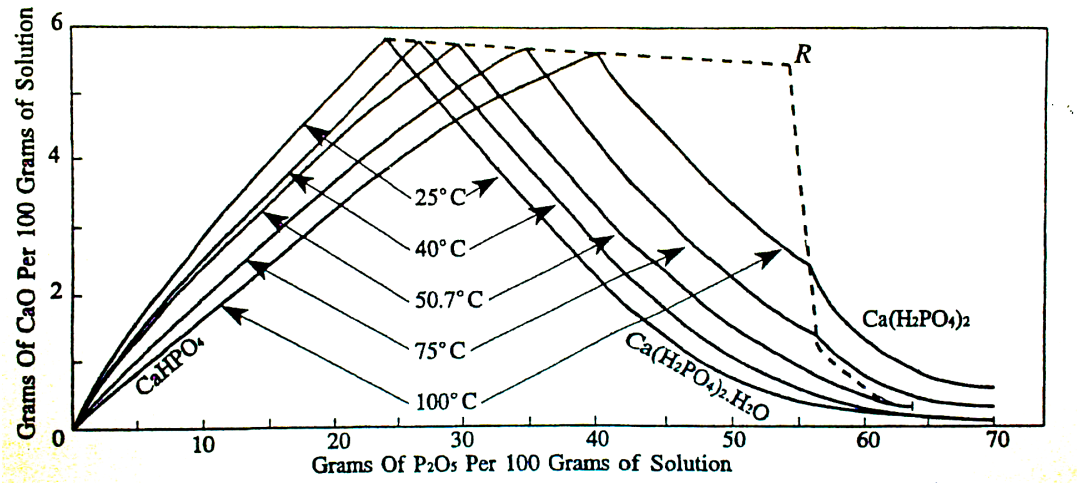

Figure 1.1: Phase diagram of CaO-P_2O_5-H_2O [11].

1.2.2 Octacalcium Phosphate (OCP)

OCP ($Ca_8H_2(PO_4)_6 \cdot 5H_2O$) occurs by the slow hydrolysis of $CaHPO_4 \cdot 2H_2O$ in CH_3COONa at a pH of 6.1. Also, it can be produced by hydrolysis of dicalcium phosphate dihydrate at 85°C in weak HNO_3 when pH is set to 5 for 30 minutes. In the decomposition procedure, OCP losses water during hydration and forms dicalcium phosphate anhydrous, HA, β-$Ca_2P_2O_7$ and tripolyphosphate [12].

OCP has a triclinic structure and its space group is P_1, in which unit cell parameters are a= 19.692 Å, b= 9.523 Å, c= 6.852 Å and α= 90.15°, β= 92.54° and γ= 108.65 ° [13].

1.2.3 Dicalcium Phosphate Dihydrate (DCPD)

DCPD ($CaHPO_4 \cdot 2H_2O$) can be produced by a direct precipitation method by the simultaneous addition during continuous stirring of a solution containing $Na_2HPO_4 \cdot 2H_2O$ and $CaCl_2 \cdot 6H_2O$ in a solution of KH_2PO_4 when pH is between 4 and 5 [6,14,15].

The structure of DCPD is monoclinic and has a P_1 space group with lattice parameters of a= 5.812 Å, b= 15.180 Å, c= 6.239 Å and β= 116° [16].

1.2.4 Dicalcium Phosphate Anhydrous (DCPA)

DCPA ($CaHPO_4$) preparation procedure is similar to the preparation of DCPD by addition of phosphate and calcium solutions to KH_2PO_4 but reactions should be occurred at 100^oC [17,18]. DCPA is less soluble than DCPD under all conditions.

DCPA has a triclinic structure at room temperature (RT), space group P_1 with lattice parameters of a= 6.910 Å, b= 6.672 Å, and c= 6.998 Å, α= 96.34^o, β= 103.82^o and γ= 88.33^o [19].

1.2.5 Anhydrous Tricalcium Phosphates (TCP)

TCP has a Ca/P ratio equal to 1.5, which is similar to Ca/P molar ratio of hydrated apatitic precipitates, so the word anhydrous is used to distinguish these compounds [20]. There are two types of TCP, which are α-TCP and β-TCP with the chemical formula of α-$Ca_3(PO_4)_2$ and β-$Ca_3(PO_4)_2$, respectively. These can be transformed to each other by changing the temperature. β-TCP is transformed to α-TCP at 1125^oC [20].

Crystalline structure of α-TCP is monoclinic and has a $P2_1/a$ space group with lattice parameters of a=12.877 Å, b= 27.280 Å, c=15.219 Å and β= 126.20 ^{o} [21]. Moreover, β-TCP has a rhombohedral structure and its space group is R3c with a unit cell parameters of a= 10.439 Å and c=37.375 Å [22].

1.2.6 Tetracalcium Phosphate (TetCP)

TetCP ($Ca_4O(PO_4)_2$) can be synthesized under anhydrous situation. It can be used as bone cement if it is mixed with DCPD or DCPA and this mixture transforms to an insoluble calcium phosphate ($Ca_4H(PO_4)_3 \cdot 5H_2O$) in the presence of

water [7]. TetCP has a monoclinic structure with a space group of $P2_1$ and its unit cell parameters are a= 7.023 Å, b= 11.986 Å, c= 9.473 Å, β= 90.90^o at 25^{o}C [23].

1.2.7 Amorphous Calcium Phosphate (ACP)

ACP ($Ca_3(PO_4)_2 \cdot 3H_2O$) can be produced at RT by the rapid addition of $Ca(NO_3)_2$ to a solution of $(NH_4)_2HPO_4$ to obtain a Ca/P molar ratio equal to 1.5. In ACP, the Ca/P ratio does not change under dry conditions while in aqueous conditions it can be transformed and crystallized to a Ca-deficient apatite [7].

1.3 Bone

Bone is a hard tissue whose duties are: maintaining the shape of the body, protecting the soft tissues, transmitting the forces during movement and acting as calcium storage in body [24].

Bone composition is 65 wt% mineral, 35 wt% organic matrix, cells and water. Bone minerals are located between collagen fiber in the form of small crystals in needles, plates and rods shapes. Bone mineral is impure HA. Impurities are carbonate, citrate, magnesium, fluoride, strontium etc. The organic matrix is composed of 90% collagen and 10% of various noncollagenous proteins which are osteocalcin, osteonectin, osteopontin and bone sialoprotein [25,26].

1.3.1 Structure of Bone

Bone has a hierarchical structure (Figure 1.2) which varies from macrostructure to nanostructure. These structures are the macrostructure that consists of compact and trabecular bone; the microstructure which consists of Haversian systems (Osteons) and Trabeculae; the submicrostructure which consists of Lamellae and Haversian canals; the nanostructure consists of collagen fiber and

the subnanostructure which consists of collagen fibril and collagen molecules [24,27].

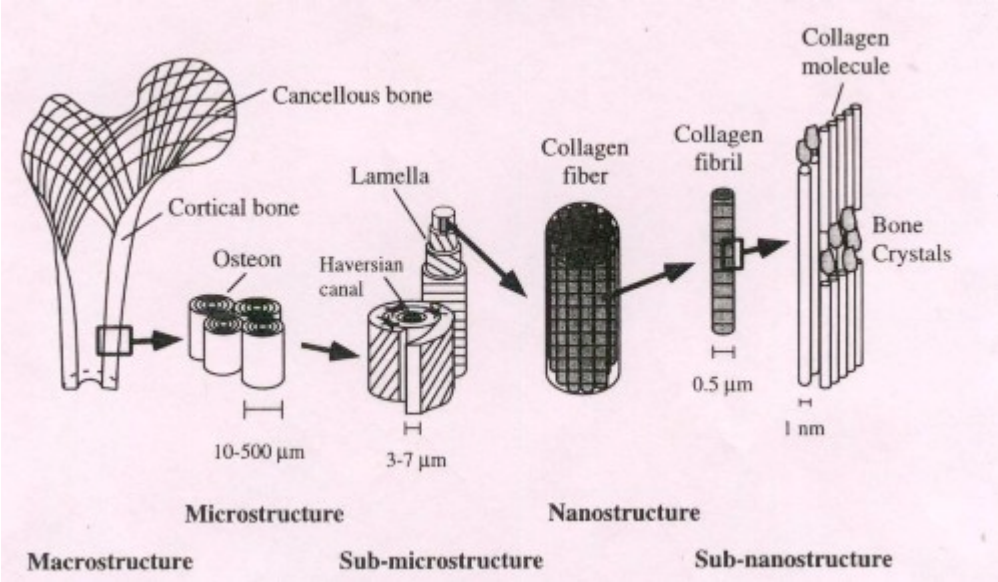

Figure 1.2: A schematic of hierarchical structure of bone [28].

1.3.1.1 Cortical and Cancellous Bones

Cortical and cancellous bones have different developing stages, architecture, function, proximity to the bone marrow, blood supply, rapidity of turnover time and age dependent changes [29].

Cortical bone is a dense, solid mass with only microscopic channels (Figure 1.3). It forms at outer surfaces of all of the bones and its duties are supporting and protecting the function of the skeleton [29].

Approximately 20 % of the skeletal mass in the adult human skeleton is cancellous bone which is a lattice of large plates and rods known as the trabecula, found in the inner parts of bones (Figure 1.4) [29]. Also, it is porous and found in the cuboidal bones, the flat bones and the ends of long bones. Its porosity varies from 75% to 95% and the pores are interconnected and filled with marrow [27].

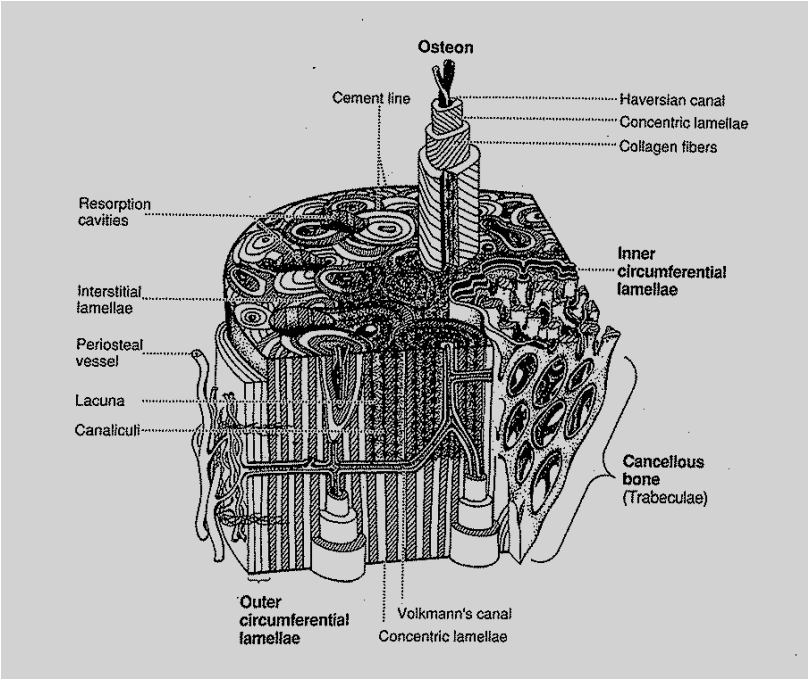

Figure 1.3: Portion of a long bone shaft [30].

1.3.1.2 Woven and Lamellar Bone

Two main types of mammalian bones are woven and lamellar bones. The bone tissue developed in embryo is woven bone. Endochondral and intramembranous ossification form cancellous woven bone. It has interwoven coarse collagen fibers matrix and osteocytes distributed more or less at random. Also, it is less organized and has short life than lamellar bone [31,32].

Lamellar bone formation is slow and highly organized. It consists of different layers, which are parallel to each other. These parallel layers are called lamellae, which are built of an anisotropic matrix of mineral crystals and collagen fibers [32].

1.3.2 Mechanical Properties of Bone

Mechanical properties of bone can be determined by determination of its density (apparent density and mineral density), porosity, microscopic structure, anisotropy and heterogeneity.

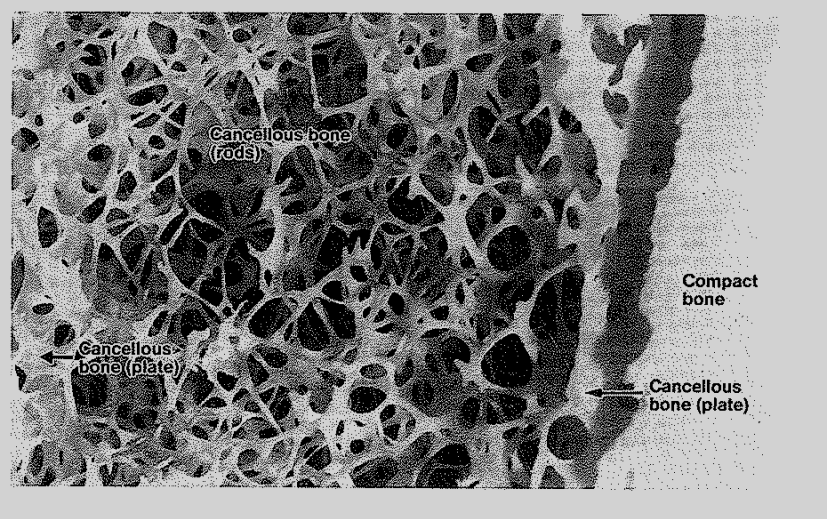

Figure 1.4: Photograph of a thick ground section of part of the proximal tibia showing the cortical and cancellous bone [30].

1.3.2.1 Bone Density

There is a relationship between density of cortical bone and both of the porosity and mineralization of the bone. Due to the structure of cortical bone, there is no difference between apparent density and material density. Average apparent density of cortical bone is approximately 1.9 g/cm^3 [33]. However, stiffness and strength of cancellous bone are a function of apparent density and mineral density. The apparent density of cancellous bone varies from 0.14 to 1.10 g/cm^3 [34].

The compressive strength of cancellous bone is in a relationship with apparent density of the bone (Equation 1.1), where σ is the strength in MPa and ρ is the apparent density [34].

$$\sigma = 60\rho^2 \qquad (1.1)$$

Also, the compressive modulus of cancellous bone has a relationship with apparent density of the bone. Figure 1.5 illustrates the correlation between apparent density and properties of cancellous bone.

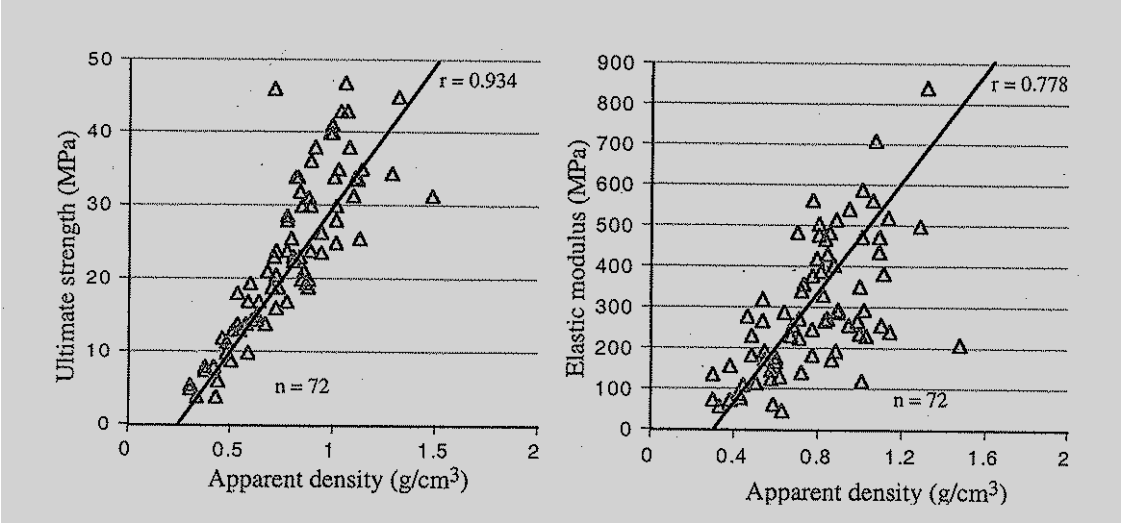

Figure 1.5: The correlation between apparent density and properties of cancellous bone [25].

1.3.2.2 Porosity

Porosity is explained as the ratio of void volume to total volume. Porosity clearly affects the mechanical properties of bone, indeed, more porous bone has a weaker mechanical strength [27,35]. Haversian canals and vascular channels are defined as pores in cortical bone, so they have a strong effect on mechanical properties of cortical bone [28]. The correlation between the porosity and the mechanical properties of a cortical bone is shown in Eq. 1.2 [28].

$$E= 33.9\ (1- p)^{10.99} \qquad (1.2)$$

Where E is the elastic modulus, (1- p) illustrates the bone volume fraction and p is the relative density.

1.3.2.3 Anisotropy and Heterogeneity

Loading directions on bone samples affect the mechanical properties of bone. Bone shows the highest elastic modulus in longitudinal direction, the lowest is in transverse direction, and the elastic modulus of specimens taken at any angles between 0 and 90^{o} have intermittent magnitudes (Figure 1.6) [25,28,35,36].

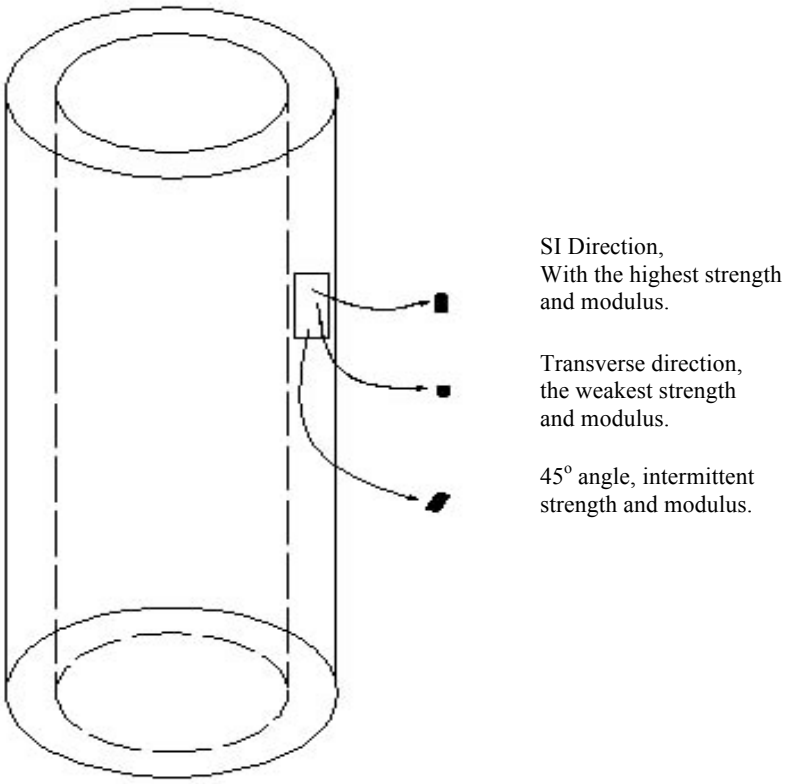

Figure 1.6: Cortical bone cylindrical specimens taken from different directions [25].

In cortical bone, collagen fibers and osteons are oriented longitudinally. Hence, it has the highest elastic modulus in longitudinal direction [28,37]. Also, cancellous bone shows anisotropic properties on its trabecular morphology [38]. In the case of cortical bone, its mechanical properties are more homogeneous along the length than around the circumference. The differences in the properties around the quadrant of cortical bone are small [39,40,41].

1.3.3 Cells, Organic and Inorganic Parts of Bone

Bone cells make up a low percentage of bone composition but this percentage is very crucial in forming and maintaining of bone matrix. There are four types of cells which are classified into two groups: cells which are cooperated in resorption process and those in form ationot bone [24,27,42].

Osteoclasts are formed by monocytes originating in the hematoposetoc of the bone marrow and cooperate in the resorption of bone. Resorption takes place throughout the length of invaginated brusb or buried border of the cell, which peripheral clear zone seal it to the bone surface [27,42]. Figure 1.7 illustrates an electron photomicrograph of a portion of an osteoclast.

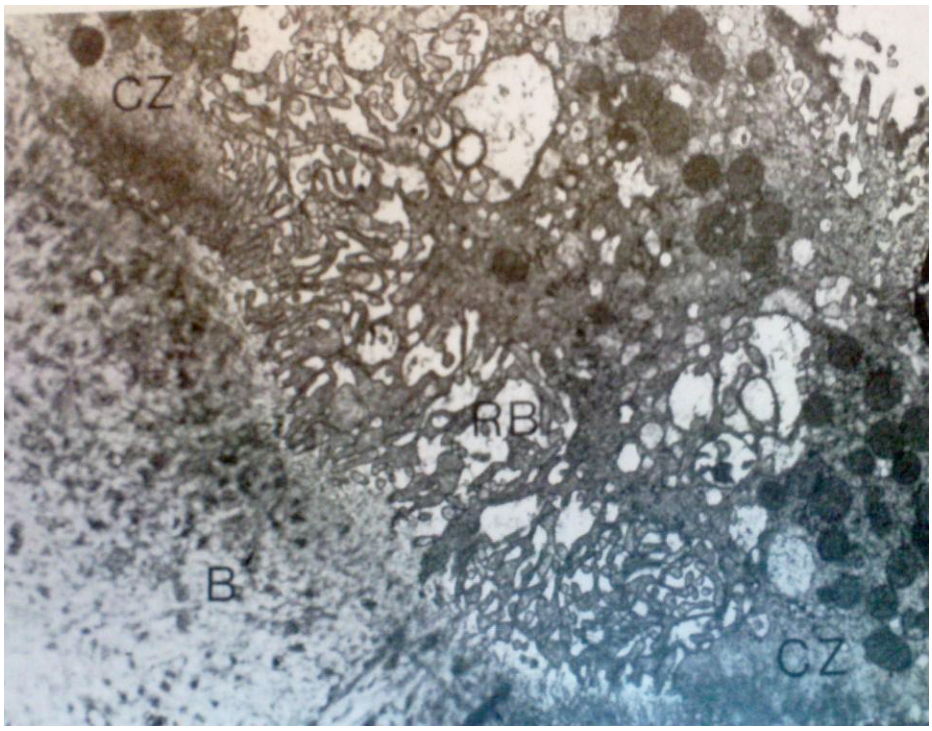

Figure 1.7: Electron micrograph of portion of an osteoclast (upper right) resorbing bone (lower left) [42].

Osteoblasts make osteoid, which is the organic portion of the bone matrix and also osteoblasts are mononuclear. Osteoid consists of collagen,

noncollageneous proteins, proteoglycans and water. During calcification high amount of the water is substituted by mineral. Mineralization or calcification front is the boundary between osteoid and calcified bone [27,42].

Figure 1.8 exhibits an electron photomicrograph of osteoblast. Dark region in the bottom shows the mineralized bone and the light region in the middle of the dark region illustrates osteoid.

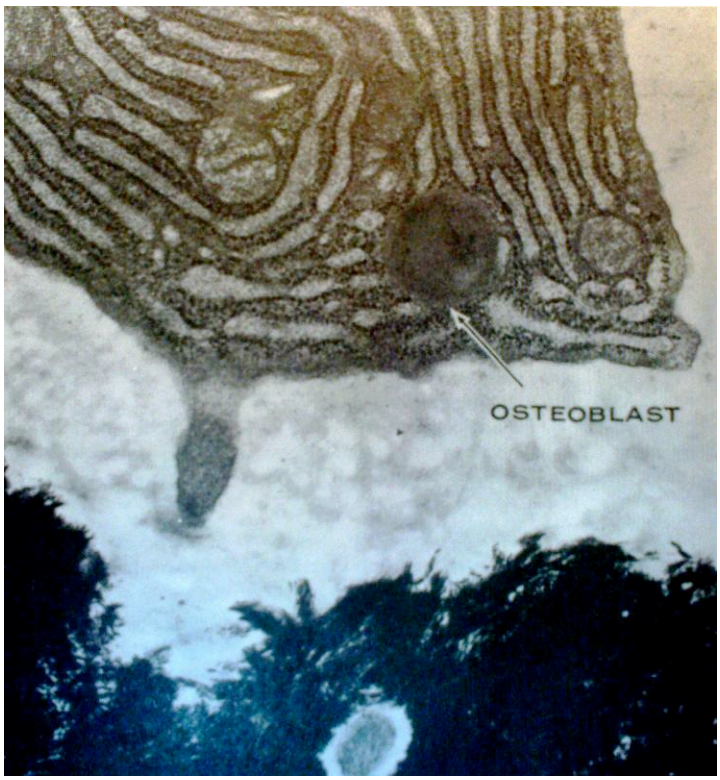

Figure 1.8: Electron photomicrograph of osteoblast forming bone [34].

Osteoblasts can be differentiated from mesenchymal cells by attending to the region, where the bone is formed. Mesenchymal cells are originated in cambium (lateral meristems) layer of the priosteal membrane or in the stromal tissue of bone marrow. Mesenchymal cells can be differentiated from osteoblast by applying mechanical loads to the tissue [27,42].

Osteocytes are earlier osteoblasts, which are interred by the osteoblasts in the bone are made in neighbors. Osteocytes sit in lacunae and combined with other osteocytes and also with osteoblasts throughout the canaliculi [27,42].

Bone lining cells are similar to osteocytes indeed these are osteoblasts which are escaped from burring in newly formed bone and maintain on the surface. Bone lining cells are inactive during bone formation and straightened against the bone surface, when bone formation is stopped but they don't have a continuous form. It is believed that they have a crucial role in the transfer of mineral into and out of bone and also sensing the mechanical strain. Also, they initiate bone remodeling in response to various chemical and mechanical stimuli [27,42].

1.3.4 Presence of Various Ions in Bone

HA is the main constituent of the mineral part of bone, which is doped with various elements. It was reported that these dopant elements affect the mechanical properties of the bone [43].

It was reported that Al^{3+} ion enters to hard tissues along with Ca so it acts as an inhibitor in forming of HA in vitro [44]. For instance, it was found that increasing of the Al amount in blood plasma cause a significant decline in bone mineral density and bone mineral content of low birth infants but this is not true for full term infants indeed it is believed that in low term infants amount of Al affects the initiation and progression of bone mineralization. However, Al accelerated the formation of osteoid [44].

Another metallic ion which is essential for mammalians is boron (B). It was found that amount of B affects the amount of vitamin D which is absorbed, so it may affect the bone metabolism [45]. In addition, another research shows B has a role in postmenopausal osteoporosis [45].

Cadmium (Cd) shows high toxicity and carcinogenicity, so these properties decrease its application. Researches show that Cd diminishes calcium absorption and increase calcium loss from bone and also decrease mineralization ability of

bone. Thus, Cd prevent self-assembly in the extracellular matrix of bone and decrease collagen production [46,47].

Mg^{2+} ion deficiency affects all stages of skeletal metabolism causing cessation of bone growth, decrease of osteoblastic and osteoclastic activities, osteopenia and bone fragility [48]. The Mg^{2+} ion content of the natural apatite is around 6 mol% but the Mg content can be changed depending on the aging. It is contained in high concentrations in the cartilage and bone tissues during the initial phases of osteogenesis and it tends to disappear when the bone tissue becomes mature [49].

Strontium (Sr) shows a metabolic behavior similar to calcium [50]. It was reported that Sr has good effects on bone such as: increasing the replication of preosteoblastic cells and including in the bone formation in cell calvarial cultures. In addition, Sr ranelate (a Sr salt) declines bone resorption [50]. Sr ranelate increases the bone strength because of increasing the bone formation and declining of resorption [50]. Therefore, Sr increases the number of osteoblasts and decreases the number of osteoclasts [50].

It was illustrated that three mechanisms determine the uptake and release of bone seeking elements. These three mechanisms are listed below [51]:

- Adsorption, which has an important role in bone metabolism and causing to an increase in mineral volume.
- Resorption.
- Surface exchange and diffuse exchange.

It was reported that Sr is taken up into bone by two different mechanisms: 1) an initial rapid mode which is depending on osteoblastic activity (ionic exchange) and 2) a slower mechanism involving the incorporation of Sr^{2+} into the crystal lattice of the bone mineral [50].

Fluoride is a trace element that affected the bone mineralization during bone formation. It was proved that the effectivity of fluoride depends on the dose of fluoride and also genetic is an important factor on effectivity of fluoride in bone

mineralization [52]. F^- stimulates osteoblastic activity and postpones mineralization of new bone are illustrated by Mousny et al. [52]. Mousny et al. showed that fluoride treatment did not have any influence on bone microarchitecture but it increases the osteoid formation and declines mineralization heterogeneity [52]. Also, fluoride ions affect the bone mechanical properties due to altering mineral-organic interfacial bonding [52].

Zinc is the first element in group 12 of periodic table. It was illustrated that zinc ion has an important role in the preservation of bone mass by stimulating osteoblastic bone formation and inhibiting osteoclastic bone resorption [53]. Wang et.al. investigated the effects of zinc on osteogenic and adipogenic differentiation of bone marrow stromal cells and the adipogenic isolated mouse primary bone marrow stromal cells and osteoblasts [53]. They illustrated that zinc supplements did not affect cell growth. However, it can affect cell growth in individual concentrations, both the osteogenic and adipogenetic differentiation of marrow stromal cells are limited by zinc ion and zinc ion depressed adipogenetic differentiation at lower concentration for osteoblasts but the effect could turn to promotion or diminished when the concentration of zinc increased [53].

1.4 Hydroxyapatite

HA is the main component of hard tissues like teeth and bone and it is widely used as a substituent of bone due to its high biocompatibility and ability in showing bioactive properties. It is able to bond to bone, so it has been widely used as a bulk implant in non-load bearing areas of the body [54,55].

HA is the most attractive among the calcium phosphates for biomedical applications because it has the most stable phase above a pH of 4.3 [56]. Also, it accelerates bone growth and bonding of bone tissue with the implant surface [57]. These properties lead to wide usage of HA in biomedical applications including matrices for drug release control and also as coatings on orthopedic implants [56,58,59]. However, it has poor mechanical properties such as low strength,

hardness and fracture toughness, which limit the application of HA to the non-load bearing areas in the body [60].

1.4.1 Structure of HA

The general formula of stochiometric HA is $Ca_{10}(PO_4)_6(OH)_2$, which has a Ca/P ratio equal to 1.67. Theoretically the structure of HA is monoclinic and space group is $P2_1/b$, in which unit cell parameters are a=9.42148 Å, b=2a, c=6.88147 Å, $\gamma=120^o$, but it is too difficult to synthesize monoclinic HA [61]. Earlier studies showed that it could exhibit the hexagonal structure with space group $P6_3/m$. Figure 1.9 illustrates the atomic structure of HA with a $P6_3/m$ space group. The large and small solid circles are phosphorous in the PO_4^{3-} group and hydrogen in the OH^- group, large and open circles show the oxygen in OH^- and PO_4^{3-} groups and double line circle exhibits the calcium ion [62].

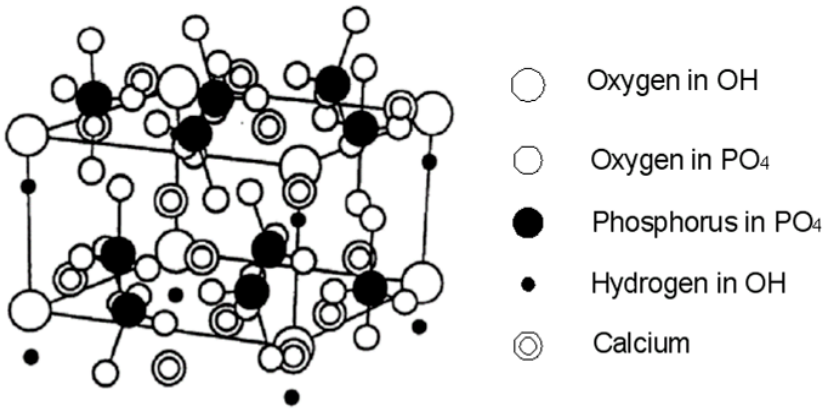

Figure 1.9: The atomic structure of HA with a $P6_3/m$ space group [62].

1.4.2 Synthesis Methods of HA

In order to synthesize HA, there are different methods such as solid state reaction, wet chemical method, precipitation method, hydrothermal reaction,

emulsion and micro-emulsion method, sol-gel method, alkoxide and other chemical methods. Some of these methods, which are widely used are explained below.

1.4.2.1 Solid State Method

In this method, HA is formed during acid reactions, first an inorganic mixture prepared by using acetone or water then it is milled, dried and heat treated [63,64]. Milling process is important because it affects the powder size of the product and also decreases the risk of contamination [64]. Heat treatment is also important because of structural transitions, which are seen during this stage [63, 64].

It was reported that HA synthesized by this method shows good mechanical properties and also good biocompatibility [64]. Materials are produced with this method exhibit higher hardness values than natural bone. However, density of them is similar to natural bone density [64].

1.4.2.2 Hydrothermal Reactions Method

In order to synthesize HA, DCPD mixed with calcium carbonate ($CaCO_3$) or calcium hydroxide ($Ca(OH)_2$) and the ratio of Ca/P should be 1 or 1.67 if the mixture is prepared with ($CaHPO_4 \cdot 2H_2O$) and ($CaCO_3$). The mixture is hydrolyzed in a NaOH and filtered to separate the aggregates. Finally, the HA powders are heat treated at various temperatures. It was reported that increasing the heat treatment temperature affected the grain size and also formed a new phase in both of the Ca/P ratio [65].

1.4.2.3 Hydrolysis Method

In this method, HA is produced by the hydrolysis of DCPD (Brushite) on the basis of following two stage reaction.

$$DCPD \rightarrow HA(Ca/P<1.67) \rightarrow HA(Ca/P=1.67) \quad (1.3)$$

The first stage of reaction causes a structural change from that of the brushite into the apatite structure, and the second stage brings only a compositional adjustment, and increases the Ca/P ratio [66].

1.4.2.4 Sol-gel Method

HA produced with sol-gel method exhibits good chemical homogenity due to a molecular level mixing of the calcium and phosphorous. Figure 1.10 exhibits the synthesis of HA with the sol-gel method [67]. It is widely used due to low processing temperature and ability to produce nanocrystalline powders [68].

It was reported that sintering time and temperature have affected the degree of crystallinity, morphology and particle size of HA in sol-gel synthesis [67].

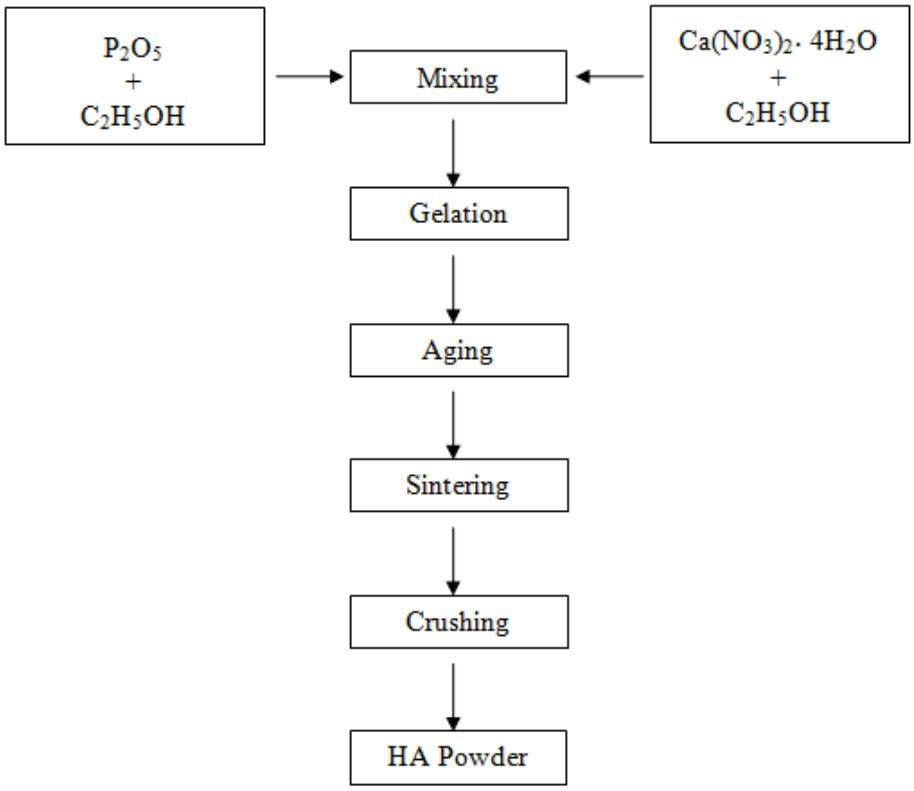

Figure 1.10: Stages of sol gel method [67].

1.4.2.5 Precipitation Method

Precipitation method is a wet synthesis method. In this method, calcium nitrate and ammonium phosphate are used as starting materials and ammonia is used to control the pH of the solution [66]. Two mixtures are prepared by using calcium nitrate and ammonium phosphate. After stirring these mixtures at 25^{o}C, di-ammonium hydrogen phosphate mixture is added dropwise into calcium nitrate and ammonium is added in order to pH adjustment [66]. The HA precipitate is removed from the solution by filtering to obtain a cake. The precipitates are dried, calcified and sintered. It was reported that in this method sintering temperature and pH of the solutions affect the grain size of the products [66].

1.4.2.6 Electro Crystallization from Aqueous Electrolytes

In this method, HA crystals were prepared by mixing a 0.042 M $Ca(NO_3)_2$ to 0.025 M $(NH_4)H_2PO_4$ in deionized water at RT [69]. Electro crystallization is a coating method. It was proved that electro crystallization is an effective method for producing bioactive HA coatings on porous and nonporous materials [69]. This method is not advised for fabricating materials with a dense coating layer [69].

1.4.3 Mechanical Properties of HA

HA has a brittle nature due to its low fracture toughness (<1 MPa·m$^{1/2}$) and low ductility [70]. In addition, mechanical properties of HA are diminished because of its decomposition to TCP [59].

Elastic modulus of HA is about 130 GPa, which is higher than that of trabecular bone (~17.50 GPa) and cortical bone (~20.55 GPa) [71,72]. High elastic modulus of HA causes a fracture at the bone and material surface because of greater stress concentration [73].

Porous structure of HA accelerates the ingrowth of bone on the interface of implant by providing a network for the ingrowth of bone and also the porous

structure affected the mechanical properties of HA [73,74,75]. It was reported that the elastic modulus and hardness of HA have an exponential relationship with porosity [73].

Several factors such as the compression pressure, sintering conditions, macroporosity and microporosity effect the mechanical properties of HA [76]. For example, compressive strength of the HA decreases with increasing the microporosity in HA [77]. Also, it was reported that sintering temperature has a direct relation with density, grain size, compressive strength and elastic modulus [76].

Fracture toughness of HA increases with an increase in sintering temperature up to 1250^{o}C [76]. However, it decreases with increasing the sintering temperature if the temperature is higher than 1250^{o}C [76]. Also, synthesis method of HA has an effect on mechanical properties because synthesis methods have an influence on grain size of HA [76].

1.4.4 Doping of Ions into HA

HA can be doped with various ions in order to improve its mechanical properties and also increase its similarity to natural bone. Some of the ions which are used for this purpose are: Mg^{2+}, Zn^{2+}, Cd^{2+}, Sr^{2+}, Ba^{2+}, Na^{+}, K^{+}, F^{-}, Cl^{-}, Y^{3+}, La^{3+}, In^{3+}, Bi^{3+}, Pb^{4+}, V^{5+} and As^{3-} [78,79, 80].

Doping of HA with various ions cause changes in lattice parameters, morphology, increased osteoblast adhesion and also decrease in grain boundary energy [81,82]. About structural properties of HA doped with Mg^{2+}, Cd^{2+}, Zn^{2+} and Y^{3+} ions, lattice parameters of doped HA decreased and also grain sizes of all doped HA were smaller than those of pure HA, except for HA doped with Cd^{2+} ions [83].

Webster et al. showed that Y^{3+}, a trivalent cation, substituted in Ca^{2+} sites and they indicated the excessive positive charge due to substitution of Y^{3+} ions are reduced by formation of a calcium ion vacancy for each yttrium ion [83]. Also, it was shown that bulk porosity of HA samples was increased by increasing the Y^{3+}

content [78]. HA doped with Y^{3+} ions shows higher osteoblast adhesion than pure HA [84]. Webster et al. investigated the adsorption of vitronectin and collagen proteins on doped and pure HA in order to prove higher osteoblast adhesion of doped HA [84]. Also, HA doped with Y^{3+} ions adsorbed greater amount of vitronectin and collagen proteins which indicate better osteoblast adhesion [84].

Mg^{2+} ions can substitute for Ca^{2+} ions in the HA structure and inhibites CaP precipitation because it is mainly adsorbed on the crystalline surface of HA [85]. Moreover, ions that are larger than Ca^{2+} ions, can substitute for calcium sites in the HA [86]. However in the case of Mg^{2+} ion substitution into HA, it is difficult to protect the phase purity. The Mg^{2+} substituted HA becomes unstable upon sintering due to the difference in the atomic radii of Mg^{2+} and Ca^{2+} ions [86]. Doping of Mg^{2+} ions into HA causes contraction in the hexagonal unit cell volume and reduction in the mean crystal size of HA [86]. Doping of 5 wt% Mg into HA resulted in mechanical properties (such as compressive strength) comparable to those of physiological bone (e.g., 170 MPa for human femur) [84,87,88]. Moreover, Al^{3+} ions decreased the grain size in comparison to pure HA and accelerated the transformation of HA to TCP and CaO [89].

Fluoride has been widely added into HA to improve its thermal stability and biological properties. Fluoride substitution in HA affects the physical and biological properties of HA [90]. F^- ions substitute for the OH^- ions in HA. If OH^- ions are partially replaced with F^- ions, the obtained material is called fluoridated-HA (FHA; $Ca_5(PO_4)_3(OH)_{1-x}F_x$, $0 \leq x \leq 1$). If OH^- ions are completely replaced with F^- ions, fluorapatite (FA; $Ca_5(PO_4)_3F$) is obtained [91, 92].

1.4.5 Biological Properties of HA

Structure of HA is similar to that of bone mineral, which accelerates the bone growth on the material [93]. Also, HA is stable under physiological pH and temperature [94]. For implants, a mixture of HA and TCP is used because it

dissolves faster than pure HA. The rate of dissolution is important in an implant because it is desirable to be resorbed by the bone after assisting the bone repair [43,95].

1.5 Tricalcium Phosphates

TCP is widely used as an implant in hard tissues due to its similarity to the inorganic part of the bone, good biocompatibility and osteoconductivity. However, it should be used in non-load bearing areas and also pure TCP is not good enough in stimulation of cell proliferation and bone formation [96,97]. It was found that β-TCP is resorbable in vivo and it is replaced with new bone growth [68]. Thus, it is suitable for applications such as periodontal bone defects repair and sinus lift which ability of quick replacing is crucial [68].

TCP has poor mechanical properties like brittleness and insufficient densification behavior. Transformation from β-TCP to α-TCP phase prevents the TCP from further densification and also expansion of the crystal unit cell volume during this phase transition causes micro-cracks in the structure, which reduces the mechanical strength of the material [98]. Since β-TCP has high solubility and biodegradation rate, it can be used as an implant on which acceleration of bone formation is necessary [68].

1.5.1 Structure of TCP

TCP has four polymorphous, which are α, α′, β and γ phase. Among TCP polymorphous, the α′ and γ phase are very difficult to prepare, because they should be prepared under high temperature and pressure [99]. Different phases can be used in different applications depending on whether a bioresorbable or a bioactive material is desired.

1.5.1.1 Structure of α-TCP

Crystal structure of α-TCP is monoclinic and space group is $P2_1/a$ with lattice parameters of a = 12.887 Å, b = 27.280 Å, c = 15.219 Å and β = 126.20^o [21]. It was reported that TCP has 24 formula units per unit cell or containing 312 atoms per unit cell (Figure 1.11) [100]. α-TCP consists of two types of ion columns located along the (010) direction. Column A consists of Ca^{2+} ions while column B consists of both Ca^{2+} and PO_4^{3-} ions [100].

1.5.1.2 Structure of β-TCP

Structure of β-TCP is rhombohedral and space group is R3c with unit cell parameters of a = 10.439 Å, c = 37.375 Å. It was reported that β-TCP has 21 formula units for one hexagonal unit cell (Figure 1.12) [22,101].

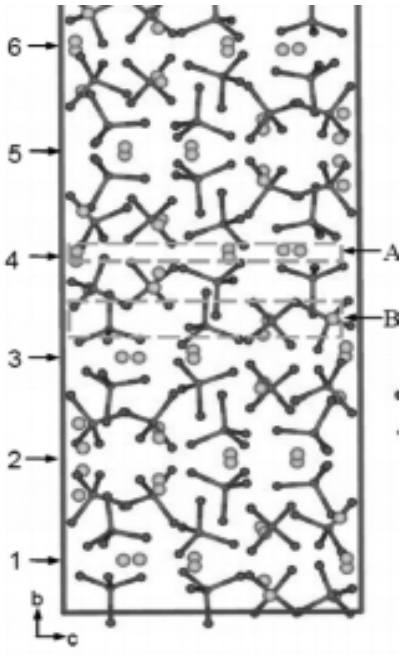

Figure 1.11: α-TCP projection along the a axis: A, Ca column; B, Ca-PO_4 column; numerals 1-6 along the left side denote the six possible cutting positions for making surface models [100].

It was reported that β-TCP in 6-Ca sites are half occupied which is shown by dashed line in Figure 1.13. Three Ca vacancies per unit cell are required in order to maintain the neutral charge of the cell but they can be distributed in different ways over the six sites [100].

1.5.2 Mechanical Properties of TCP

β-TCP is widely used as an implant due to its higher resorbability in vivo with new bone compared to other biomedical materials. However, low mechanical strength limits the application of β-TCP. It was reported that the mechanical strength of ceramics depends on density, grain size, grain morphology and grain boundary characteristics [103].

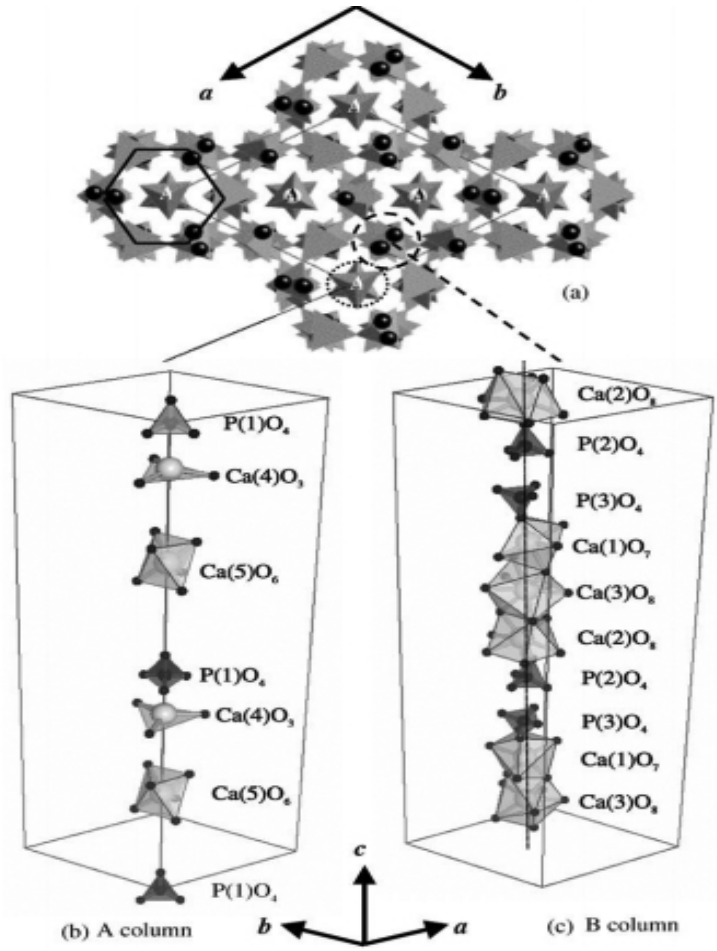

Figure 1.12: a) Projection of the crystal structure of β-TCP on the (001) plane, showing the A and B columns. 'A' denotes the A column, while no indication is given for B column. The rhombus in (a) denotes the hexagonal unit cell of β-TCP. (b) and (c) are the configuration of CaO_n and PO_4 in the A and B columns [102].

The effect of nano-size and micron-size powders on the sintering, microstructure, mechanical strength and degradability of the β-TCP bioceramics was investigated by K. Lin et al. [103]. Materials with nano-size powders had higher density and mechanical strength and also, fine grain size at low sintering temperatures [103]. Mechanical properties of biaphasic calcium phosphate as a function of their microporosity, macroporosity or combination of microporosity and macroporosity were studied [104].

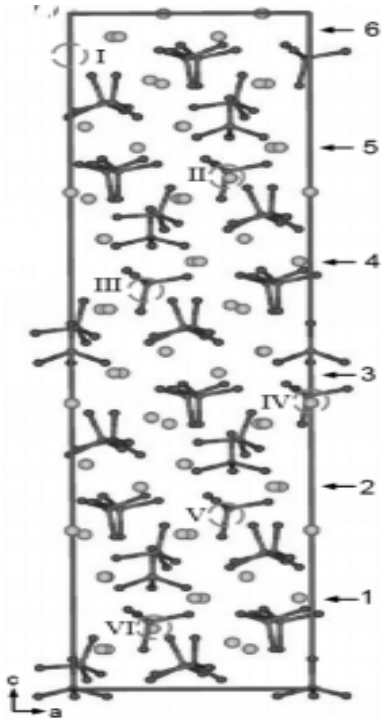

Figure 1.13: β-TCP project along the b-axis and dashed circles denote six half occupied Ca sites; numerals 1-6 along the right side denote six possible cutting positions for making surface models [100].

De Groot described the changes of mechanical strength of HA and TCP as a function of total porosity (0-50%) and microporosity (0-5%) [105]. Bignon et al. used exponential rules in order to describe the changes of biphasic CaPs compressive strength as a function of macroporosity [106].

Numerous types of models were previously stimulated in order to describe the effect of microporosity and macroprosity on mechanical properties of TCP [104]. One of these stimulations is homogenization, in this method, it was assumed that mechanical properties of porous ceramics are equal to zero and this assumes lead to polynomial homographic laws. In these phenomena, the morphology of

porosity was assumed as a composite microstructure which is made of two solid phases. This model cannot be used in porous materials which were obtained by the incomplete sintering of a pressed powder, because it was assumed that mechanical strength is equal to zero, when the pore volume fraction is equal to one [104]. For example, Gibson and Ashby used a finite element model in order to exhibit elastic modulus dependence on relative density [107].

The acceptable method is a model described by Le Huec [108]. This model defined the impact of microporosity (from 22% to 39% of the specimen volume occupied by pores smaller than 100 μm in diameter) and macroporosity (from 0% to 28% of the specimen volume occupied by pores larger than 100 μm in diameter) to compressive strength of HA using empirical polynomial regressions. One of the weakness of this model is narrow range of the microporosity while it was proved that the microporosity range is higher than 20 % of the total volume and also in this model only the compressive fracture stress was considered. Maybe the weakest point of this model is that there are not enough experimental data to prove this hypothesis [104].

F. Pecqueux et al. investigated the influence of microporosity and macroporosity on the mechanical properties of biphasic CaP bioceramics (modeling and experiment) [104]. The materials which are used in this research are the mixture of β-TCP and HA with the wide range of microporosity and macroporosity. Mechanical properties like Young's modulus, compressive strength and fracture toughness were measured and compared to previously proposed analytical models and hypothesis [104]. The theory is used for describing their model. The model considers that given the huge difference in size between macropores (hundreds of micrometers) and micropores (micrometers), the materials can be regarded as a quasi-continuous microporous "matrix" containing isolated macropores. In this respect, it becomes possible to split the respective influence of macroporosity and microporosity (Figure 1.14). In particular, in the case of the Young's modulus, this is written as [104]:

$$E = E_0 \cdot f_1(p\ macro) \cdot f_2(p\ micro) \qquad (1.3)$$

Where, E: the Young's modulus of the porous material; E_0: the value for a fully dense body [104].

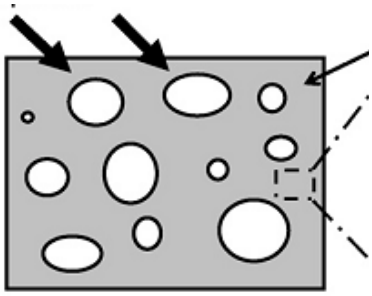

Figure 1.14: Scanning electron micrographs and schema of biaphasic CaP porous structure [104].

Since its mathematical formulation is well adapted to the case of isolated pores within continuous matrix, it is equal to zero only when the material is fully porous. For a material with a porosity p, the elastic modulus is [104]:

$$E = E_m \cdot (1- p)^m \quad (1.4)$$

In this case, the "matrix" between macropores is itself microporous, and its local Young's modulus, E_m: reduced by the presence of micropores compared to the bulk value, E_0. The above equation becomes [104]:

$$E = E_m \cdot (1- p_{macro})^m \quad (1.5)$$

E_m is therefore the Young's modulus of a microporous ceramic whose porosity results from incomplete sintering of a pressed powder.

They used a model published by Wegh et al. in order to stimulate the fracture toughness [109]:

$$K_{IC} = K_{IC0} \cdot [N_C \cdot (1- p_{micro}) - (N_C-1) \cdot (1-p_{micro})^{2/3}] \cdot (1- p_{macro})^m \quad (1.6)$$

K_{IC0} is the toughness of a fully dense material, so p_{micro} is equal to p_{macro}=0.

Also, it is known that brittle materials are affected by flaws and flaws can cause a great decrease in mechanical properties [76]. As a conclusion they illustrated that the presence of macropores strongly affects the critical flaw size but the latter appears to increase with macroporosity. This phenomenon can be

explained by presence of clusters of macropores which are acting as critical flaws, becoming larger as macroporosity increases [104].

1.5.3 Doping of Ions into TCP

TCP is widely used as an implant or coatings on metallic prosthesis due to its good biocompatibility and osteoconductivity. Also, TCP ceramics are used as an implant because of non-toxicity, antigenically inactivity, non-carcinogenicity and bond directly to bone without intervening to connective tissue [110]. However, it cannot be used in load bearing areas and also it does not cooperate in bone formation [111]. However, it was reported that TCP shows good bioactivity after doping with some trace elements [111]. Trace elements such as Mg and Si are widely used as dopant elements in TCP ceramics. Si increases bone formation in vivo, so TCP ceramics doped with silicon are used as biodegradable materials which enhance the rate of bone regeneration [110].

It was reported that Sr and Mg in TCP has a great role in new bone growth. It was illustrated that Sr promotes osteoblast function and subsequent bone formation and in low percent increases the replication of preosteoblastic cells and also enhances bone mineralization. While high dose of Sr decreases bone mineralization [112]. Doping of CaPs with Mg is widely studied because of its qualitative changes in bone matrix and also affected the mineral metabolism [112].

1.5.3.1 Doping of F^- Ions into TCP

F^- ions are positioned on OH^- sites in TCP [90]. It was reported that fluoride decreases the solubility/ degradation in CaPs because of its high acidity resistance and also can promote bone regeneration [113].

Seeley and coworkers investigated the effects of doping of TCP with NaF and CaO [113]. They found that doping of ions into TCP increases the density of

doped TCP [113]. Density of TCP doped with 2% NaF shows 15% increase and also there are considerable increase in density of TCP doped with 2% NaF and 0.5% Ag_2O. It was proved that combination of liquid phase formation in grain boundaries and substitutional defects lead to an increase in the sintered density of TCP [106]. Grain size of doped samples are increased in comparison to pure TCP due to two phenomen which are liquid phase formation in the grain boundries and substitutional defects [113]. It was clearly proved that pure TCP has more porous structure than TCP which is doped by NaF [113].

Also, they exhibited that there are not a significant difference between β-TCP peaks of different compositions which means that there are not clear alterations in main phase of these ceramics due to addition of dopants [106]. However, α-TCP and HA peaks show a little change [113]. For example, NaF samples show considerable reduction in α-TCP phase formation and this can be happened because NaF crystal structure is more similar to crystal structure of β-TCP [113].

1.5.4 Biological Properties of TCP

TCP has higher resorption rate than HA, good biocompatibility and osteoconductivity [114]. β-TCP is used for bone repair because it can be easily replaced by growing bone upon implantation [112]. While degrading in the host, TCP is replaced by the regenerating bone and acts as a seed for the new bone and as a supplier of the Ca^{2+} and PO_4^{3-} ions [115]. TCP is more degradable than HA, which shows minimum degradability properties; preventing the bone ingrowth for extended periods [116]. Because of the higher resorption rates of TCP, strength reduction occurs in the bone- implant interface. Therefore, the dissolution behavior of TCP should be controlled by chemical modifications. Doping of TCP with trace elements such as Mg is used in controlling the dissolution behavior of TCP and also stabilizing the β-TCP phase at high temperatures above 1125˚C [103,115].

It has been reported that TCP ceramics do not show cytotoxic properties on contact with extract fluids (a liquid preparation of a vegetable drug) [76]. Also, it has been observed that the amount of TCP particles and particle size strongly affect osteoblast behaviour [76]. Although, large amounts of small particles negatively affect the cell growth and cause cell death, small amount of α-TCP has a positive effect on osteoblast proliferation and expression due to the release of mineral ions such as calcium and phosphate [76]. β-TCP may cause a cell death because of the formation of intramitochondrial Ca-P crystals [76]. However, this phenomenon is rarely reported. It has been reported that doped TCPs improve osteoblast attachment and proliferation [76].

1.6 Aim of the Study

The aim of this study is to investigate the microstructural and mechanical properties of TCP doped with Al^{3+} and/or F^- ions. TCPs were synthesized by precipitation method and sintered at 1100 ^oC for 1 and 5 h. Density measurements of the samples were determined by Archimedes method. X-ray diffraction (XRD) and Fourier transform infrared spectroscopy (FTIR) analysis were used in order to investigate the presence of phases and bonds. Also, scanning electron microscopy (SEM) was used for investigation of the microstructure of the samples. In order to investigate the mechanical properties of samples, microhardness and diametral strength tests were applied.

CHAPTER 2

2. MATERIALS AND METHODS

2.1 Materials

2.1.1 Precursor Materials

Chemicals used for the synthesis of TCP were calcium nitrate ($Ca(NO_3)_2 \cdot 4H_2O$) and di-ammonium hydrogen phosphate ($(NH_4)_2HPO_4$) (Merck, Germany). In the synthesis of fluoride and aluminum doped TCPs, aluminum nitrate ($Al(NO_3)_3 \cdot 9H_2O$) and ammonium fluoride (NH_4F) (Sigma-Aldrich, USA) were used. Also, ammonia (NH_4OH) solution (Merck, Germany) was used in order to adjust the pH of solutions during the synthesis.

2.2 Synthesis Methods of TCP

2.2.1 Synthesis of Pure TCP

TCP powders were synthesized by precipitation method. Calcium nitrate tetra hydrate ($Ca(NO_3)_2 \cdot 4H_2O$) and di-ammonium hydrogen phosphate ($(NH_4)_2HPO_4$) were used as main precursors. These precursors were added to distilled water in order to prepare 0.6 M ($Ca(NO_3)_2 \cdot 4H_2O$) and 0.4 M $(NH_4)_2HPO_4$. This molar amount of precursors were used because the Ca/P ratio was aimed to be 1.5. Ammonia was added into the di-ammonium hydrogen phosphate solution after stirring for one hour. After stirring for 10 minutes, ammonia and calcium nitrate solutions were added drop wise into the di-ammonium hydrogen phosphate-ammonia mixture. Ammonia was used in order to adjust the pH of the final mixture to 11-12. The final mixture was heated until boiling during stirring to accelerate the reaction. After this stage, the mixture was stirred for one night. After mixing the

solution overnight, the mixture was filtered with a fine filter paper to obtain a wet cake. The wet cake was dried in the furnace at 200°C to remove the excess water. After drying, the samples were sintered at 1100°C for 1 and 5h.

2.2.2 Synthesis of Doped TCPs

In addition to the main precursors used in the synthesis of pure TCP, aluminum nitrate ($Al(NO_3)_3 \cdot 9H_2O$) and ammonium fluoride (NH_4F) were used to obtain aluminum and fluoride doped TCPs. 13 different compositions of pure and doped TCPs were prepared. Descriptions of pure and doped TCP samples according to their aluminum and fluoride ion compositions are summarized in Table 2.1.

The synthesis procedure of the doped TCPs were the same as the procedure for pure TCP synthesis. Aluminum nitrate was added into the calcium nitrate tetra hydrate solution and ammonium fluoride was added into the di-ammonium hydrogen phosphate solution. After the two solutions were mixed with the same procedure, the final mixture was stirred, filtered, dried at 200°C and sintered at 1100°C for 1 and 5 h.

2.3 Characterization Methods

2.3.1 Structural Analysis

2.3.1.1 Density

Density of sintered materials were measured by Archimedes method. Dry weights of the materials were measured in order to obtain the weight of the materials and then weight of the materials were measured in water. The differences between amount of the weight in water and dry weight gave the volume of the discs. Thus, densities of the materials were calculated according to this formula:

d = dry weight / (dry weight – weight in water) (2.1)

Table 2.1: Description and compositions of pure and doped TCPs.

Sample ID	**Mole % Al^{3+}**	**Mole % F^-**
TCP	0	0
TCP0.5Al	0.5	0
TCP1Al	1	0
TCP2.5Al	2.5	0
TCP5Al	5	0
TCP0.5F	0	0.5
TCP1F	0	1
TCP2.5F	0	2.5
TCP5F	0	5
TCP0.5Al,0.5F	0.5	0.5
TCP2.5Al,1F	2.5	1
TCP2.5Al,2.5F	2.5	2.5
TCP2.5Al,5F	2.5	5

Finally, relative densities of the materials were calculated by comparing the measured densities with the theoretical density of pure TCP.

2.3.1.2 X-Ray Diffraction Analysis

XRD was used to investigate the presence and amount of the phases and lattice parameters of the samples by using a Rikagu DMAX 2200 machine. XRD was performed on the samples with Cu-Kα radiation at 40 kV/40 mA. The samples were scanned from 20 to 70 with 2Θ angles with a scan speed of 2.0^{o}/min. Results which were obtained from XRD were compared with Joint Committee on Powder Diffraction Standards (JCPDS) in order to determine the positions of the diffracted planes.

2.3.1.2.1 Rietveld Analysis

Rietveld analysis refinement was conducted by means of the General Structure Analysis System (GSAS) computer program, in order to detect the phase peaks more exactly and the weight fraction of the phases. Also, the lattice parameters can be found by GSAS program.

The refinement was applied in several stages. The background terms for histogram 1 were setted as shifted Chebyschev (type 1) function and profile terms were setted as pseudo-Voight, a linear combination of a Lorentzian and a Gausian (type 2) function. The bumpy background was fitted by using the shifted Chebyschev function. First of all, all of the damping values were adjusted to 8, the scale factor and background were refined before any profile refinements for single phase. Then, refinements of the other parameters such as profile and cell parameters followed. In this stage, the atomic parameters of second phase were added. The sacale factor was adjusted to 1 and un-flagged, and the instrumental profile parameters (G_U, G_V, G_W) were copied to the profile information of second phase. Constraints were added for these parameters. The profile refinement was continued by selecting the parameters of the both phases at same time. Finally, cell parameters, the atomic coordinates, thermal parameters and the occupancy factor of the atoms for both of the phases were refined.

2.3.1.2.2 Lattice Parameter Measurements

β-TCP has a rhombohedral structure. The lattice parameters of β-TCP were expressed in the hexagonal form and they were calculated by successive approximation method. The unit cell volume of HA and β-TCP were calculated by the following formulas [117]:

$$V = 2.589 \cdot \left(a^2\right) \cdot c \qquad (2.2)$$

$$V = 0.866 \cdot \left(a^2\right) \cdot c \qquad (2.3)$$

Where: V ($Å^3$) is the volume of unit cell; a and c are the lattice parameters of hexagonal structure in angstrom.

According to the Bragg's equation, lattice parameters were calculated by the following formulas [117]:

$$a_0 = \left(\frac{\lambda}{2\sin\theta}\right)\sqrt{\left(\frac{4}{3}(h^2 + hk + k^2) + \left(\frac{a}{c}\right)^2 l^2\right)} \qquad (2.4)$$

$$c_0 = \left(\frac{\lambda}{2\sin\theta}\right)\sqrt{\left(\frac{4}{3}\left(\frac{c}{a}\right)^2 (h^2 + hk + k^2) + l^2\right)} \qquad (2.5)$$

where; a_0 and c_0: the calculated lattice parameters; λ: x-ray wavelength; θ: the Bragg angle for corresponding (hkl); a/c ratio: the last calculated ratio in successive approximation method. Equation 2.4 was used for the calculation of 'a' values, in which the term "$\frac{4}{3}(h^2 + hk + k^2)$" was larger than "$\left(\frac{a}{c}\right)^2 l^2$". In addition, Equation 2.5 was used for the calculation of 'c' values for the conditions, where "$h^2 + hk + k^2$" term was less than the value of "l^2".

2.3.1.3 Scanning Electron Microscopy

The average grain size of the sintered samples was determined by SEM analysis method. A SEM analysis was performed by a QUANTA 400F at a voltage of 20 kV. Firstly, the sintered samples were embedded in epoxy mold and then

polished on papers with grid from 200 to 1200. Then samples were coated with gold and platinum under vacuum. The intercept method was performed in order to determine the grain size of the sintered samples [118].

$$G_{av} = \frac{L}{N * M} \tag{2.6}$$

Where; G_{av}: Average grain size; L: circumference of the circle; N: number of the intersections along the intersection line; M: magnification.

2.3.1.4 Fourier Transform Infrared Spectroscopy

Presence of bonds in the samples were investigated by FTIR. Firstly, the samples were crushed into powders by the use of a mortar and pestle. Produced ceramic powders were mixed with potassium bromide (KBr) with a weight ratio of 1/300. In order to obtain transparent pellets, the obtained powder mixture was cold pressed. The spectra records were performed from 4000 cm^{-1} to 400 cm^{-1} using 512 scan by BioRad FTS 175 C.

2.3.2 Mechanical Tests

2.3.2.1 Vickers Micro-hardness

The Vickers micro-hardness measurements were performed by a Vickers micro hardness tester (HMV-2, Shimadzu, Japan). The samples were first polished with SiC papers (Buehler Ltd., USA) from 200 to 1200 grades and then they were polished with a 1μm monocrystalline diamond suspension (Buehler Ltd., USA). Approximately 10 measurements were performed on each sample with a diamond indenter at 200 g load for 20 seconds. The average μ-hardness was calculated by the formula below:

$$HV = 0.001854 \frac{P}{d^2} \tag{2.7}$$

Where; HV: Vickers hardness (GPa); P: Applied load (N); d: diagonal indent length (mm).

2.3.2.2 Diametral Strength

The diametral tensile strength of sintered disks was performed by a universal testing machine (LS 500; Llyod Instruments, UK). In order to measure the diametral tensile strength, disks were located between two flat plates and compression was applied by a cylinder with a speed of 3 mm/min. During the compression, a maximum tensile strength was generated across the flat surface diameters of the disks normal to the loading direction. The tensile strength of the samples were calculated with the following formula [119,120]:

$$S = \frac{2F}{(\pi \cdot D \cdot t)} \tag{2.8}$$

where: F: failure force; D: sample diameter; t: sample thickness.

CHAPTER 3

3. RESULTS and DISCUSSION

3.1 Density of the Samples

Densities of the materials sintered at 1100^{o}C are presented in Table 3.1. It was observed that densities of the most materials were increased by extending the sintering time from 1 to 5h as seen in Table 3.1.

Table 3.1: Density of pure and doped TCPs sintered at 1100^{o}C for 1 and 5h.

Group No.	Sample ID	Density (g/cm^3) 1h	Relative Density (%) 1h	Density (g/cm^3) 5h	Relative Density (%) 5h
1	TCP	2.64	85.9	2.8	91.2
2	TCP0.5Al	2.92	95.1	2.93	95.4
	TCP1Al	2.79	90.8	2.88	93.8
	TCP2.5Al	2.99	99.3	2.65	86.3
	TCP5Al	2.90	94.4	2.76	89.9
3	TCP0.5F	2.99	99.3	2.88	93.8
	TCP1F	2.92	95.1	2.94	95.7
	TCP2.5F	2.64	85.9	2.80	91.2
	TCP5F	2.80	91.2	2.94	95.7
4	TCP0.5Al,0.5F	2.98	97.0	2.82	91.8
	TCP2.5Al,1F	2.88	93.8	2.84	92.5
	TCP2.5Al,2.5F	2.91	94.7	2.89	94.1
	TCP2.5Al,5F	2.88	93.8	2.93	95.4

Although densities of Al^{3+} doped samples (TCP0.5Al and TCP1Al) increased with increasing the sintering time from 1 to 5h, densities of Al^{3+} samples (TCP2.5Al and TCP5Al) with high Al^{3+} contents decreased with increasing the sintering time from 1 to 5h. However, there was no relationship between the relative density and the Al^{3+} content after the sintering for 1h. Sample TCP2.5Al had the highest density after the sintering for 1h.

Also, it was observed that TCP0.5F has the highest density among the samples doped with F^- ions but increasing the amount of F^- ions led to decrease in density of the samples doped with only F^- ions after the sintering for 1h. These results exhibited a consistency with investigation, which proved that incorporation of F^- ions decrease the density of the materials [121]. Theoretical densities of HA and β-TCP are 3.156 and 3.07 g/cm^3, respectively.

It was reported that doping of calcium phosphates with F^- ion causes a decrease in density of products due to reduction of decomposition rate of the synthesized materials by formation of FHA (fluorapatite) which shows high thermal and chemical stability at the sintering temperatures [121].

It was reported that the relative density of pure and doped HAs was increased by increasing the sintering temperature. However, there is not a significant difference in densities of doped HA with respect to temperature. Indeed, all of the samples show a very high density after the sintering. Also, tendency was a decrease in relative density of doped HAs by increasing amount of dopants [140].

As seen in Group 3, density of materials was reduced by increasing F^- concentration except for TCP5F.

The samples which were doped with Al^{3+} and F^- ions at same time, density of the samples were generally decreased by extending the sintering time. While, density of TCP2.5Al,5F increased by extending the sintering time. Among these samples, TCP0.5Al,0.5F which was sintered for 1 h shows the highest density.

3.2 Structural Analysis

3.2.1 XRD Analysis

XRD patterns of the samples were used to investigate the presence of phases in the samples.

XRD patterns of TCP sintered at 1100 ^oC for 1 and 5h are presented in Figure 3.1. According to Figure 3.1, the XRD patterns of the samples are matched

with the JCPDS file #9-432 for HA and also the secondary phase β-TCP (JCPDS #9-169). Also, it can be found that extending the sintering time from 1 to 5h did not contribute to a major difference in peak heights of HA and β-TCP. Narrow peaks for both of the samples indicate that they were highly crystalline. Although the stoichiometric Ca/P ratio for TCP is 1.5, in our samples, we had TCP and HA biphasic materials which had a Ca/P ratio of 1.5 in the starting chemicals. This was probably occurred because of the synthesis method (precipitation method) we used, which involves high pH values during the mixing of solutions. Additionally, other parameters such as aging time and temperature can make contribution to presence of phase in the final product [122].

Also, it was reported that in the precipitation method, β-TCP can not be synthesized directly [123]. Indeed, the product is a calcium deficient apatite which decomposes to β-TCP after a heat treatment above 750^{o}C [123].

Previous studies showed that the probability of observing second phases such as TCP was increased by increasing the sintering time [124]. Thus, it can be said that the nucleation of secondary phase will be easier by increasing the sintering time because they have enough time for nucleation and growth. However, there was not a major difference in the presence of phases for the samples after the sintering for 1 and 5h as seen in Figure 3.1.

Rietveld analysis was applied on XRD data in order to detect the phase peaks more exactly and volume fraction of both phases. With the aid of GSAS program, it was found that the main phase of TCP which is sintered for 1h, is HA (61%) while the second phase is β-TCP with 39 %. While, the main phase of TCP which is sintered for 5h is β-TCP with 55 % and the second phase is HA. It is possible to say that the product is HA which decomposes to β-TCP after a heat treatment. This result is in correlation with the investigation of Douard et al. [123].

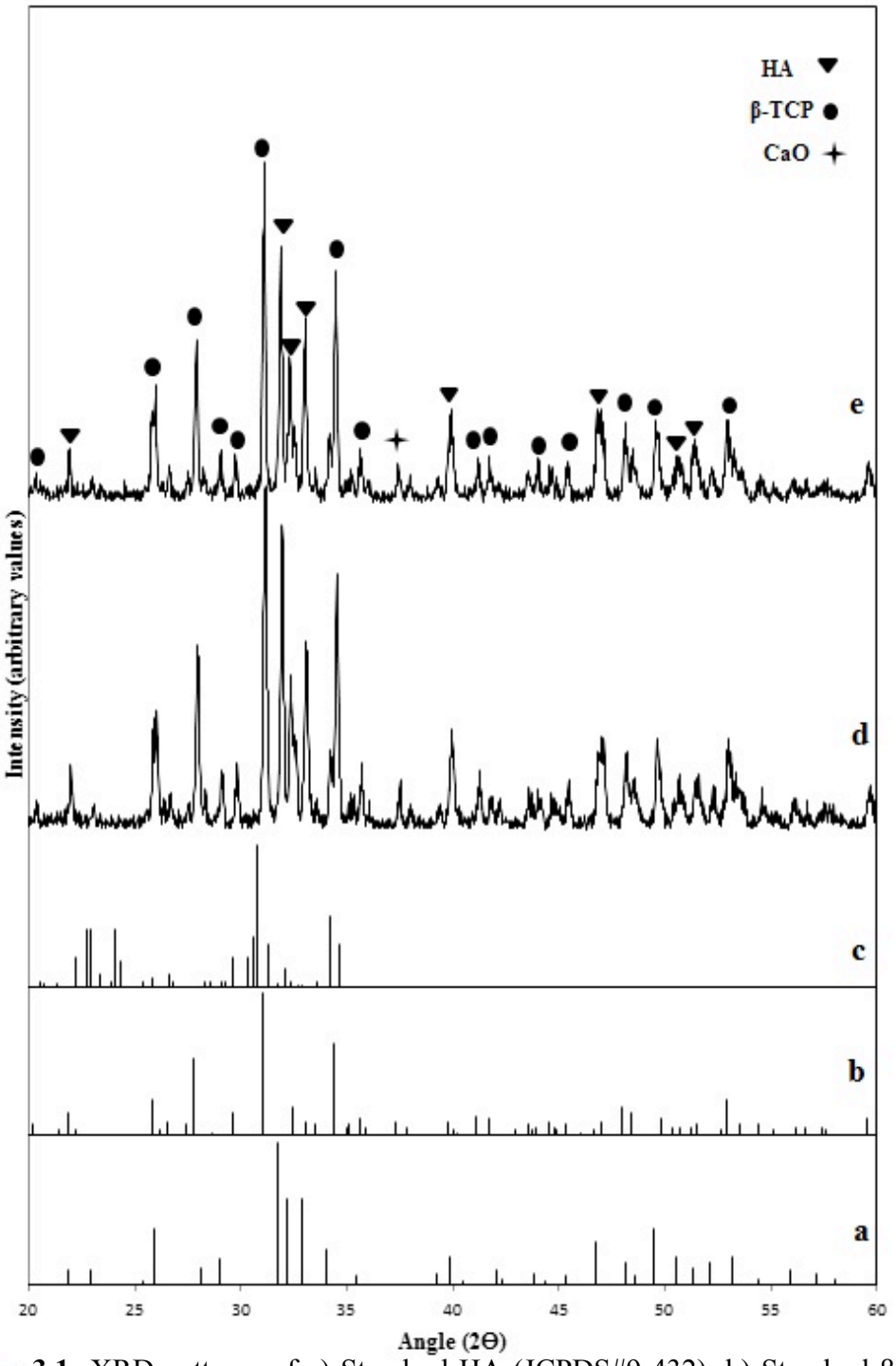

Figure 3.1: XRD patterns of a) Standard HA (JCPDS#9-432); b) Standard β-TCP (JCPDS#9-169); c) Standard α-TCP (JCPDS#9-348); d) TCP (sintered for 1h); e) TCP (sintered for 5h).

Although, addition of Al^{3+} ions into TCP does not change the XRD patterns of the samples and there are still match with the standard JCPDS file for β-TCP (Figure 3.2). This result is in correlation with investigation of Basar et al. which shows that doping of HA with Y^{3+} and F^- did not cause severe fluctuation in XRD pattern [140]. For all of the samples, secondary phases matched with XRD pattern of HA can be found. Narrow peaks show that increasing the Al^{3+} content increases the crystallinity of the samples. Also, it is clear that intensity of TCP picks increase with increasing the amount of Al^{3+} ions. It was proved that doping of Al^{3+} ions into HA accelerates its decomposition to α and/or β-TCP but for this purpose an optimal content of Al^{3+} should be used [63]. Thus, Al^{3+} ions promote the formation of TCP.

According to Table 3.2 which shows the weight fraction of the samples only doped with Al^{3+}, TCP5Al sintered for 5h has the highest percent of TCP. It was seen that the percentage of β-TCP was increased by increasing Al^{3+} ion content so it is possible to say that Al^{3+} accelerates decomposition of HA to β-TCP. Thus, an optimal content of Al^{3+} should be used in order to accelerate the decomposition of HA to β-TCP.

Table 3.2: Presence of HA and TCP phases in Al doped TCPs sintered at 1100°C for 1 and 5h.

Sample ID	Wt. Fraction of TCP 1h sintered	Wt. Fraction of HA 1h sintered	Wt. Fraction of TCP 5h sintered	Wt. Fraction of HA 5h sintered
TCP0.5AL	0.538	0.462	0.547	0.453
TCP1AL	0.618	0.382	0.644	0.356
TCP2.5AL	0.859	0.141	0.874	0.126
TCP5AL	0.961	0.039	0.985	0.015

The XRD patterns of the samples which are doped by F^- ions (Figure 3.3), are matched with the standard JCPDS files for HA and also β-TCP but they indicated that peaks were shifted right by adding F^- ions. Also, it was clearly shown that intensity of peaks increased by increasing the amount of F^- ions. Also, peaks get narrower in higher amount of F^- ions, so it increases the degree of crystallinity.

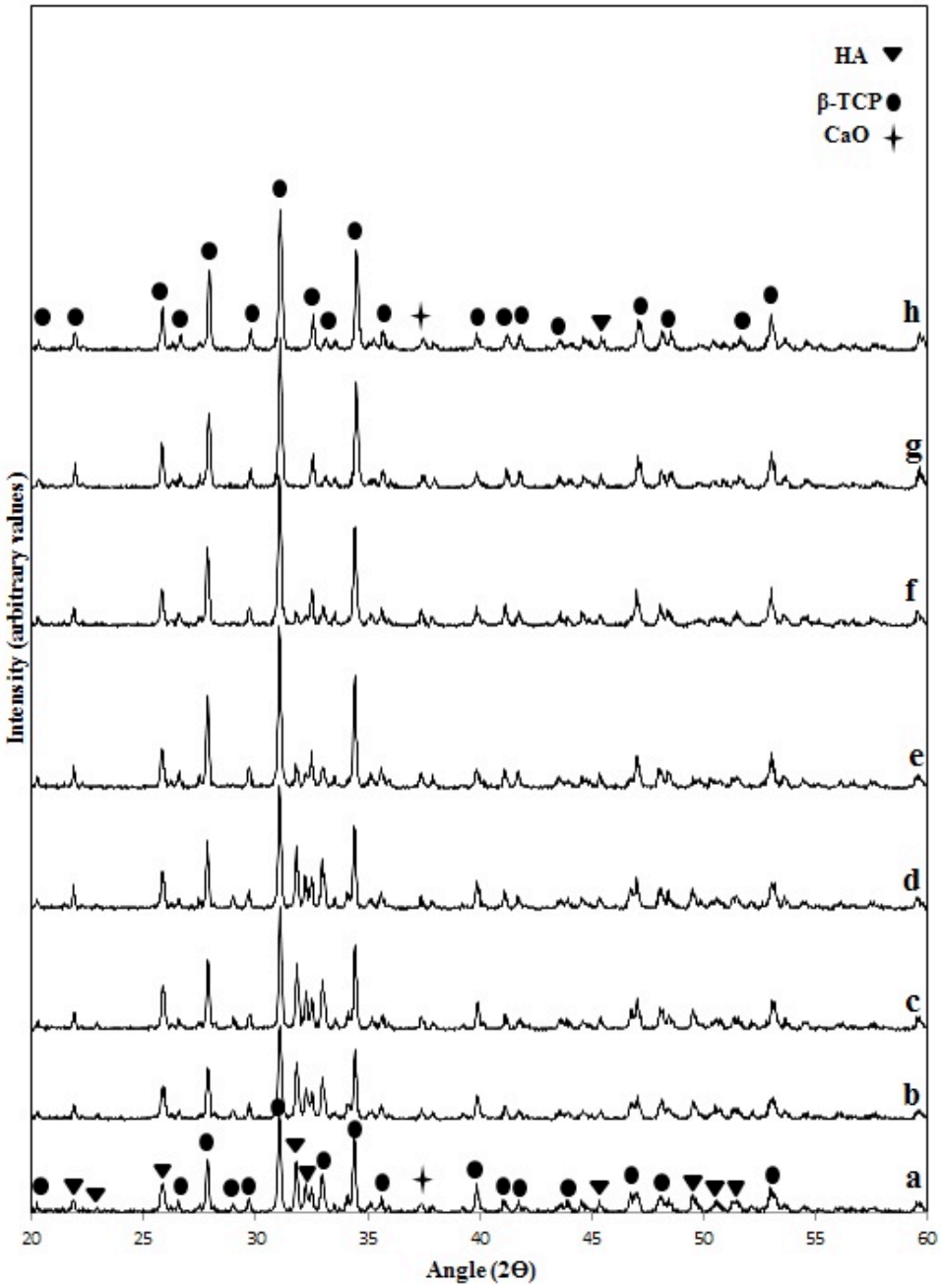

Figure 3.2: XRD patterns of a) TCP0.5Al (sintered for 1h); b) TCP0.5Al (sintered for 5h); c) TCP1Al (sintered for 1h); d) TCP1Al (sintered for 5h); e) TCP2.5Al (sintered for 1h); f) TCP2.5Al (sintered for 5h); g) TCP5Al (sintered for 1h); h) TCP5Al (sintered for 5h).

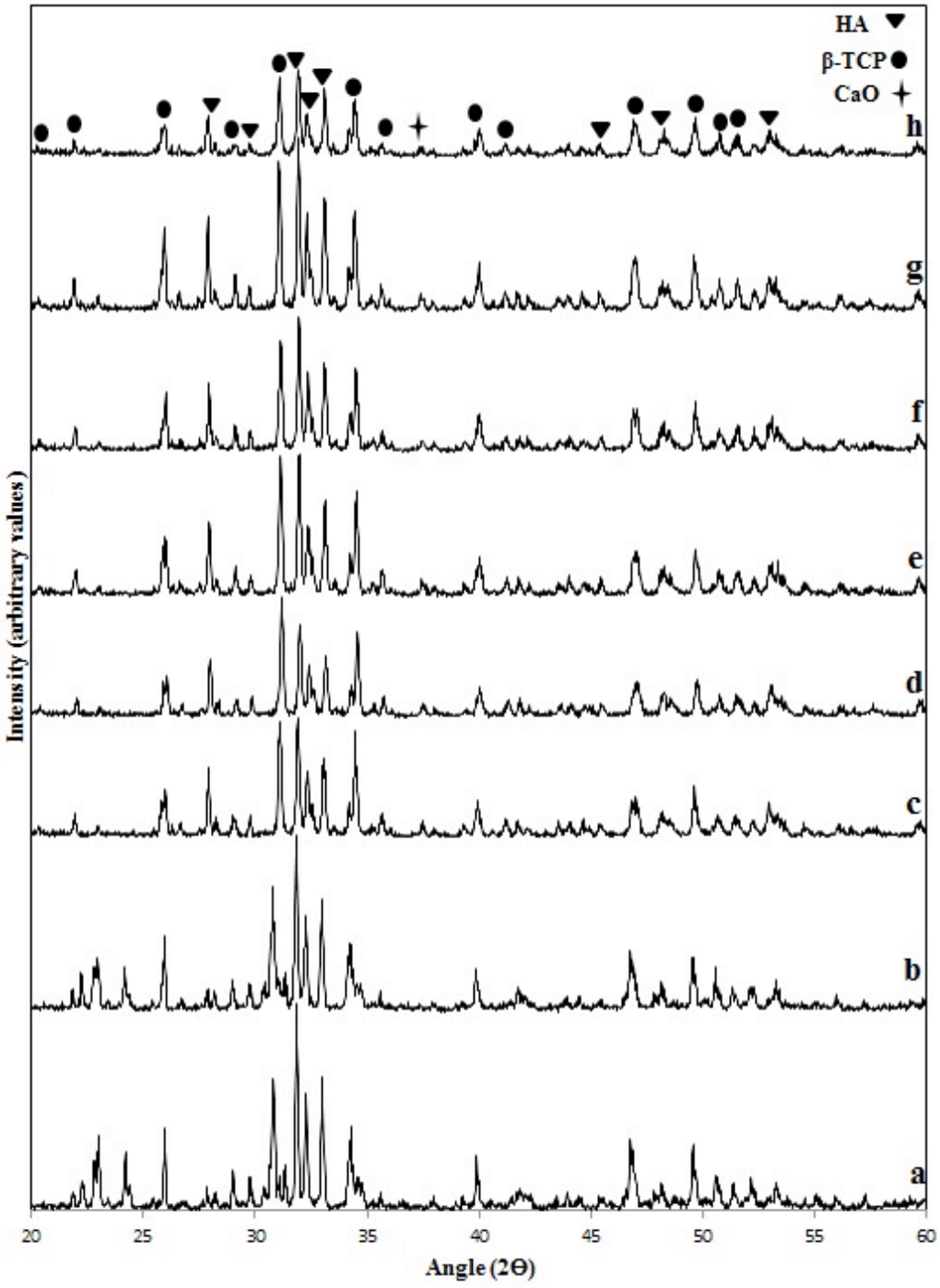

Figure 3.3: XRD patterns of a) TCP0.5F (sintered for 1h); b) TCP0.5F (sintered for 5h); c) TCP1F (sintered for 1h); d) TCP1F (sintered for 5h); e) TCP2.5F (sintered for 1h); f) TCP2.5F (sintered for 5h); g) TCP5F (sintered for 1h); h) TCP5F (sintered for 5h).

It was reported that addition of F^- ions improves the structural stability of calcium phosphates [125]. It was also reported that as a result of F^- ion doping into apatite lattice, peak shift to higher 2θ values were observed in the position of (211), (300) and (112) planes in an increasing manner with an increase in F^- ions content [126,127]. While, this investigation showed that there is no relation between F^- content and the position of (211) and (300) planes position. Thus, shift of these peaks is independent from the amount of F^- ions. This contrast is approved by previous studies of Okazaki et al. [126,127].

The wt. fractions of F^- doped samples clearly show that the percentage of β-TCP phase was increased by extending the sintering time as seen in Table 3.3. This phenomena is in correlation with the investigation of Douard et al.[123]. In the precipitation method the initial product is a calcium deficient apatite which decomposes to β-TCP after a heat treatment. Indeed, extending the sintering time accelerates the decomposition of HA to β-TCP. Additionally, these results proved that an optimum amount of F^- ions should be used in order to accelerate the decomposition of HA to β-TCP.

Table 3.3: Presence of HA and TCP phases in F doped TCPs sintered at 1100°C for 1 and 5h.

Sample ID	Wt. Fraction of TCP 1h sintered	Wt. Fraction of HA 1h sintered	Wt. Fraction of TCP 5h sintered	Wt. Fraction of HA 5h sintered
TCP0.5F	0.502	0.498	0.521	0.479
TCP1F	0.523	0.477	0.552	0.448
TCP2.5F	0.558	0.442	0.579	0.421
TCP5F	0.420	0.580	0.495	0.506

Figure 3.4 shows the XRD patterns of the samples doped with both Al^{3+} and F^- ions. The XRD patterns in this figure clearly show that all of the samples are biphasic materials and the XRD patterns of these samples are matched with the standard JCPDS files for β-TCP and HA. It was shown that the intensity of peaks of the samples increased by increasing the sintering time and F^- content. This increase

in intensity of peaks might indicate an increase in crystallinity of these samples because it was reported that F^- ions improve the crystallinity of the apatite structure [121]. Moreover, percentage of HA was increased by increasing the F^- ions content [121].

The presence of HA in the structure of β-TCP which is used in biomaterial applications does not act as an inhibitor [129]. According to ASTM F 1088-87 standard, the β-TCP with minimum purity of 95% and up to 5% HA is acceptable for biomaterial applications [122]. Also, it was reported that bioactivity of β-TCP increases when mixed with HA [122].

According to Table 3.4, weight fraction of β-TCP is decreased by extending the sintering time in the samples doped with both Al^{3+} and F^- ions. Also, the percentage of β-TCP decreased by increasing F^- ions content which is in correlation with investigation of Gross et al. which shows that increasing amount of F^- ions has negative effect an decomposition of HA to β-TCP [121]. Also, it is possible to say that the formation of fluorohydroxyapatite (FHA) decrease rate of formation of β-TCP because of its high chemical and thermal stability [137]. While, an increase in Al^{3+} ion content causes a great increase in wt. fraction of β-TCP. Thus, these result proved effect of Al^{3+} ions in decomposition of HA to β-TCP. In this group, TCP2.5Al,1F which sintered for 1h is more acceptable for biomedical applications according to ASTM F 1088-87 standard [122].

Table 3.4: Presence of HA and TCP phases in Al and F doped TCPs sintered at 1100^{o}C for 1 and 5h.

Sample ID	Wt. Fraction of TCP 1h sintered	Wt. Fraction of HA 1h sintered	Wt. Fraction of TCP 5h sintered	Wt. Fraction of HA 5h sintered
TCP0.5Al,0.5F	0.510	0.490	0.498	0.502
TCP2.5Al,1F	0.823	0.177	0.818	0.182
TCP2.5Al,2.5F	0.760	0.240	0.635	0.365
TCP2.5Al,5F	0.610	0.490	0.465	0.535

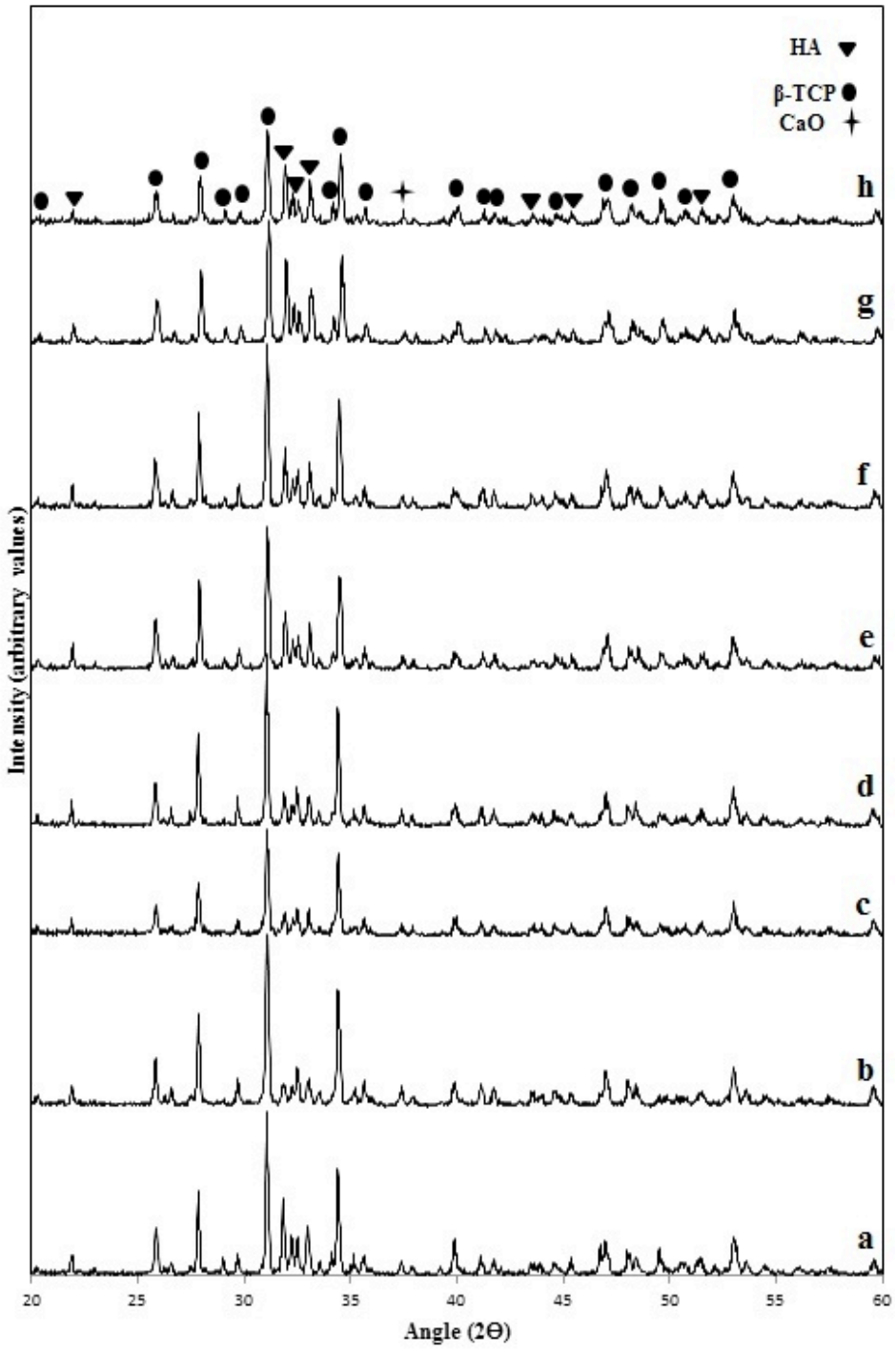

Figure 3.4: XRD patterns of a) TCP0.5Al,0.5F (sintered for 1h); b) TCP0.5Al,0.5F (sintered for 5h); c) TCP2.5Al,1F (sintered for 1h); d) TCP2.5Al,1F (sintered for 5h); e) TCP2.5Al,2.5F (sintered for 1h); f) TCP2.5Al,2.5F (sintered for 5h); g) TCP2.5Al,5F (sintered for 1h); h) TCP2.5Al,5F (sintered for 5h).

According to Table 3.5, the intensity of TCP peaks in Group 2 was increased by extending the sintering time. Thus, increasing the sintering time accelerates the decomposition of HA to TCP. Also, the intensity of TCP peaks was increased by increasing the Al^{3+} content. Therefore, Al^{3+} accelerates the decomposition of HA.

Table 3.5: The highest intensities of pure and doped TCPs sintered at 1100^{o}C for 1 and 5h.

Group No.	Sample ID	TCP Intensity 1 hour	HA Intensity 1 hour	TCP/HA 5 hour	TCP Intensity 5 hour	HA Intensity 5 hour	TCP/HA 5 hour
1	TCP	243	215	1.13	241	181	1.33
2	TCP0.5Al	153	153	1	169	95	1.78
	TCP1Al	363	363	1	370	184	2.01
	TCP2.5Al	474	474	1	491	108	4.54
	TCP5Al	439	439	1	480	96	5
3	TCP0.5F	220	346	0.64	209	294	0.71
	TCP1F	194	198	0.98	200	154	1.30
	TCP2.5F	232	237	0.98	184	223	0.82
	TCP5F	250	288	0.87	132	144	0.92
4	TCP0.5Al,0.5F	390	185	2.11	409	91	4.50
	TCP2.5Al,1F	256	60	4.26	411	54	7.61
	TCP2.5Al,2.5F	342	140	2.44	390	117	3.33
	TCP2.5Al,5F	292	193	1.51	310	144	2.15

In Group 3, intensity of TCP peaks was decreased by extending the sintering time, so it is possible to say that F^{-} ion stabilizes the HA phase. However, in Group 4, intensity of TCP peaks were increased by extending the sintering time.

3.2.1.1 Lattice Parameters

Lattice parameters, unit cell volume and change in the unit cell volume of the samples with respect to that of β-TCP are presented in Table 3.6.

It was observed that in Group 1, both of the lattice parameters were decreased by extending the sintering time and also, a decrease was observed in unit cell volume as seen in Table 3.6.

According to Table 3.6, the 'a' and 'c' lattice parameters of TCP decreased due to doping of TCP with Al^{3+} ions. We expect to see a decrease in the lattice parameters because of differences of the ionic size of Al^{3+} and Ca^{2+} ions. The ionic size of Ca^{2+} ions (1 Å) is approximately two times bigger than that of Al^{3+} (0.53 Å) is, so substitution of Al^{3+} ions in the place of Ca^{2+} ions can cause a decrease in the lattice parameters of Al doped TCPs. The lattice parameters of Group 2 were not in correlation with amount of Al^{3+} ions. Also, for each Al^{3+} ion concentration, there was a decrease in 'a' and 'c' lattice parameters as the sintering time increased.

It was reported that, β-TCP has five sites which are crystallographically independent. These independent sites are Ca(1), Ca(2), Ca(3), Ca(4) and Ca(5). The Al^{3+} ions can be substituted in these sites in different situations [130].

It was proved that ionic radii of substitution ions have significant effect in lattice parameters. For example, it was observed that substitution of cations such as Cd^{2+}, Zn^{2+}, Mg^{2+} and In^{3+} which have smaller radii than Ca^{2+} reduce the lattice

Table 3.6: Lattice parameters of β-TCP phase of pure and doped TCPs sintered at 1100°C for 1 and 5 h.

Group No.	Sample ID of 1h Sintered	a(Å)	c(Å)	V(Å^3)	ΔV(Å^3)	Sample ID of 5h sintered	a(Å)	c(Å)	V(Å^3)	ΔV(Å^3)
1	TCP	10.4106	37.4238	3512.5	0	TCP	10.3637	37.2510	3464.8	-47.7
2	TCP0.5Al	10.3762	37.2092	3469.3	-43.2	TCP0.5Al	10.3462	37.1892	3459.4	-53.1
	TCP1Al	10.3713	37.1744	3462.8	-49.7	TCP1Al	10.3713	37.1657	3461.9	-50.6
	TCP2.5Al	10.3694	37.1900	3462.9	-49.6	TCP2.5Al	10.3685	37.1898	3462.3	-50.2
	TCP5Al	10.3621	37.2486	3463.5	-49	TCP5Al	10.3598	37.0143	3440.0	-72.5
3	TCP0.5F	10.3761	37.3120	3478.8	-33.7	TCP0.5F	10.3710	37.2889	3473.2	-39.3
	TCP1F	10.3661	37.2120	3462.8	-49.7	TCP1F	10.3610	37.1989	3458.2	-54.3
	TCP2.5F	10.3650	37.2509	3465.7	-46.8	TCP2.5F	10.3696	37.2527	3468.9	-43.6
	TCP5F	10.3654	37.2305	3464.1	-48.4	TCP5F	10.3626	37.2398	3463.1	-49.4
4	TCP0.5Al, 0.5F	10.3791	37.4681	3495.4	-17.1	TCP0.5Al, 0.5F	10.3878	37.4724	3501.6	-10.9
	TCP2.5Al, 1F	10.3722	37.1913	3464.9	-47.6	TCP2.5Al, 1F	10.3715	37.1946	3464.8	-47.8
	TCP2.5Al, 2.5F	10.3645	37.2510	3465.4	-47.1	TCP2.5Al, 2.5F	10.3547	37.3114	3464.4	-48.1
	TCP2.5Al, 5F	10.3386	37.2698	3449.8	-62.7	TCP2.5Al, 5F	10.3299	37.2890	3445.8	-66.7

parameters of TCP [60,78,83]. While, substitution of cations with larger radii than Ca^{2+} ions resulted in an increase in lattice parameters [60,78,83]. These investigations show that ionic radii of substitutions have a significant effect in lattice parameters.

Lattice parameters of Group 3 in Table 3.6 clearly showed that extending the sintering time causes a decrease in the lattice parameters of β-TCPs which were doped with F^- ions except for TCP2.5F. Also, other samples of this group which were doped with F^- ions showed a tangible decrease in both 'a' and 'c' lattice parameters. It is expected that doping of TCP with F^- ions causes shrinkage in unit cell volumes because ion size of F^- ion is smaller than that of OH^- ion. The effective ionic radius of F^- is 1.33 Å while the ionic radius for OH^- is 1.37 Å [129]. It was reported that both of the lattice parameters decrease with increasing fluoride ion concentration and also, the reaction temperature has a significant effect on 'a' and 'c' axis dimension [136].

The samples of Group 4 clearly show that lattice parameters were decreased by extending the sintering time except for TCP2.5Al,2.5F. Also, it was observed that doping of TCP with Al^{3+} and F^- ions at same time lead to a decrease in lattice parameters of samples in comparison with pure TCP but it is clear that both of lattice parameters show a significant reduction with increasing the F^- ions. So that, TCP 2.5Al,5F has the smallest 'a' and 'c' among the other samples of this group. While, TCP 2.5Al,1F shows the highest increase of 'a' lattice parameter among of all of the samples. It was proved that OH^- ions are located along the 'c' axis at the center of Ca^{2+} triangles, so substituted F^- ions lie along the 'c' axis [60]. Also, F^- ions are more electronegative than OH^- ions [121]. Thus, increasing the F^- content may lead to an increase in electronegativity difference between F^- ions and Ca^{2+} ions. As a result, the attraction between Ca^{2+} and F^- ions increases. Therefore, the distance between these ions decreases which leads to a decrease in 'a' axis.

According to Table 3.7, in Group 1 both of the lattice parameters decrease by extending the sintering time from 1 to 5h.

In Group 2, the volume of unit cell of samples which sintered 1h is decreased by increasing Al^{3+} ion content. The biggest decreases in lattice parameters were observed in TCP2.5Al (5h sintered).

According to results of Group 3, the 'a' lattice parameters were decreased by increasing F^- ions content but the 'c' lattice parameters show an increase by increasing F^- ions content. A decrease in lattice parameter proved the formation of FHA in the samples [137]. It was reported, the 'a' lattice parameter of the fluoride doped samples was smaller than pure HA but the 'c' lattice parameter didn't change after substitution of F^- ions [138]. This decrease in the volume of unit cell proved that the synthesized apatite is solid solution. Also, it shows that OH^- groups of HA have been substituted by F^- ions [138]. According to Vegard's law, there is a relationship between the lattice parameter of solution and the atomic percent solute percent [139]. Thus, it could be said that there is a linear proportional relationship between the amount of substituted ions and alteration of lattice parameters [139]. It could be concluded from the Vegard's law, in Group 3 of Table 3.7, the number of hydroxyl group substituted by F^- ions increased by increasing F^- ion concentration.

The samples of Group 4 clearly show that 'a' lattice parameters were decreased by increasing F^- ions content but the 'c' lattice parameters were increase for all of the samples which sintered 1h. However, the unit cell volume of all of the samples were increased by increasing the F^- ions content and extending sintering time.

Table 3.7: Lattice parameters of HA phase of pure and doped TCPs sintered at 1100^{o}C for 1 and 5 h.

Group No	Sample ID of 1h Sintered	a(Å)	c(Å)	V(Å^3)	ΔV(Å^3)	Sample ID of 5h sintered	a(Å)	c(Å)	V(Å^3)	ΔV(Å^3)
1	TCP	9.4495	6.9045	1596.1	0	TCP	9.4362	6.8935	1589.1	-7
2	TCP0.5Al	9.4343	6.8935	1588.5	--7.6	TCP0.5Al	9.4321	6.8935	1587.7	--8.4
	TCP1Al	9.4319	6.9021	1589.6	-6.5	TCP1Al	9.4118	6.8883	1579.7	-16.4
	TCP2.5Al	9.4348	6.8875	1587.3	-8.8	TCP2.5Al	9.4321	6.8875	1586.4	-9.7
	TCP5Al	9.4345	6.8861	1586.8	-9.3	TCP5Al	9.4289	6.8798	1583.5	-12.6
3	TCP0.5F	9.4421	6.8901	1590.3	-5.8	TCP0.5F	9.4388	6.8935	1590.0	-6.1
	TCP1F	9.4328	6.8889	1586.9	-9.2	TCP1F	9.4301	6.8871	1585.6	-10.5
	TCP2.5F	9.4315	6.8976	1588.5	-7.6	TCP2.5F	9.3753	6.8570	1560.4	-35.7
	TCP5F	9.4275	6.9055	1588.9	-7.2	TCP5F	9.4231	6.9069	1587.8	-8.3
4	TCP0.5Al ,0.5F	9.4215	6.8914	1583.7	-12.4	TCP0.5Al ,0.5F	9.4200	6.8998	1585.1	-11
	TCP2.5Al ,1F	9.4315	6.9014	1589.4	-6.7	TCP2.5Al ,1F	9.4308	6.9033	1589.6	-6.5
	TCP2.5Al ,2.5F	9.4280	6.9092	1590.0	-6.1	TCP2.5Al ,2.5F	9.4247	6.9153	1590.3	-5.8
	TCP2.5Al ,5F	9.4123	6.9052	1594.1	-2	TCP2.5Al ,5F	9.4176	6.9834	1603.5	-7.4

3.2.2 Fourier Transform Infrared Spectroscopy

FTIR was applied to identify the presence of the bonds in pure and doped TCPs. The reference frequencies of calcium phosphates are given in Table 3.8.

Table 3.8: The assignment and frequencies of FTIR bands in CaPs.

Assignment	Infrared Frequency (cm^{-1})	Ref. #
OH^- (stretching)	3571.6	131
OH^- (librational)	631.7	131
Adsorbed water	~3300-3600	131
$\upsilon_4PO_4^{3-}$ (O-P-O) bend	571,611	131
$\upsilon_3PO_4^{3-}$ (P-O) stretch	1092 and 1040	131
$\upsilon_2PO_4^{3-}$ (O-P-O) bend	~462-474	131
$\upsilon_1PO_4^{3-}$ (P-O) bend	961	131
OH- F bond	~ 720 and 3570	132,133

The FTIR spectra for the samples categorized in four groups are shown in Figures 3.5 to 3.8. According to Figure 3.5, the bands for PO_4^{3-} group in 571 cm^{-1} which assigned to υ_4, the triply degenerated O-P-O bending mode and in 990-1099 cm^{-1} which are assigned to υ_3, the triply degenerated asymmetric P-O stretching mode. The OH^- stretching is visible at 3572 cm^{-1} which is coming from HA. Also, the broad band of low intensity peaks is clearly visible in the range of 4000 to 3500 cm^{-1}. Thus, it is possible to say that trace amount of water incorporated into the structure of the samples [131].

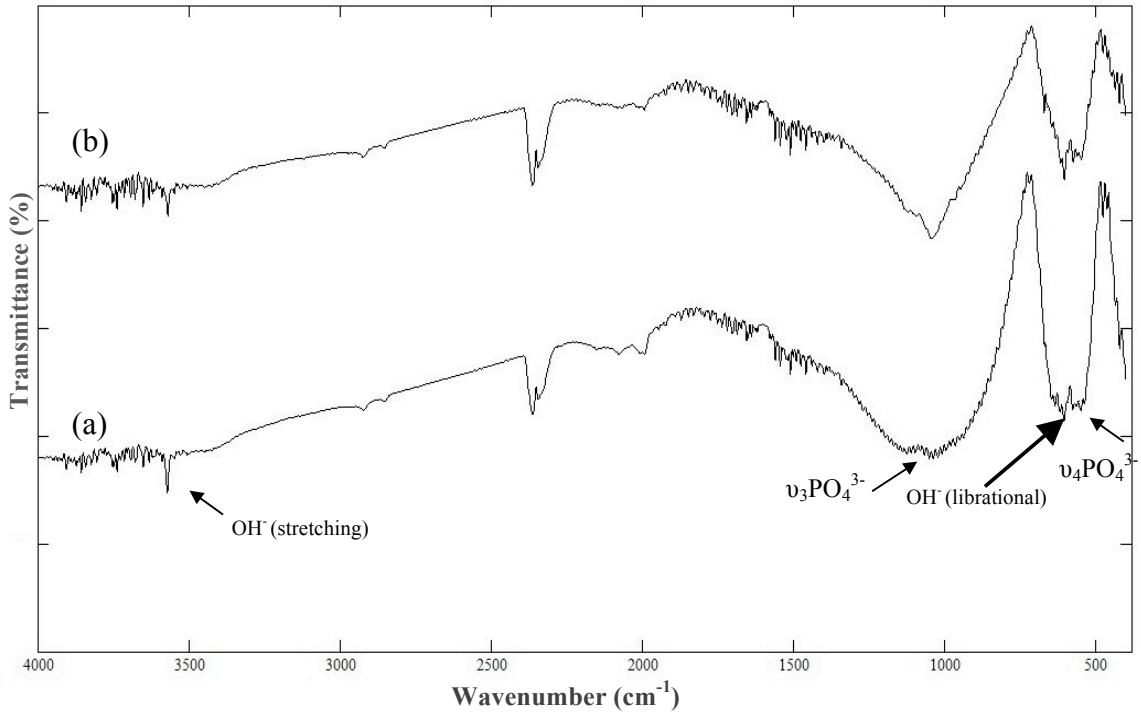

Figure 3.5: FTIR patterns of a) TCP (sintered for 1h); b) TCP (sintered for 5h).

According to Figure 3.6, samples of Group 2 the OH^- stretching and libration band which come from HA were disappeared by increasing the Al^{3+} ion content, which was in good agreement with the findings of Slosarczyk et. al. [131]. Thus, the transmittance intensities of OH^- bands decrease as the Al^{3+} ion content increase because Al accelerates the decomposition of HA to β-TCP. In addition, there are not any visible peak between 3300 and 3600 cm^{-1}. Therefore, the transformation from CaO to $Ca(OH)_2$ generally did not occur for the Al doped samples. This transformation just occurred in the TCP5Al which was sintered for 5 h. It was reported that the presence of CaO in material which use as an implant is so harmful due to its high reactivity against water [131]. The variation of OH^- bands give us quantitative information about HA and β-TCP.

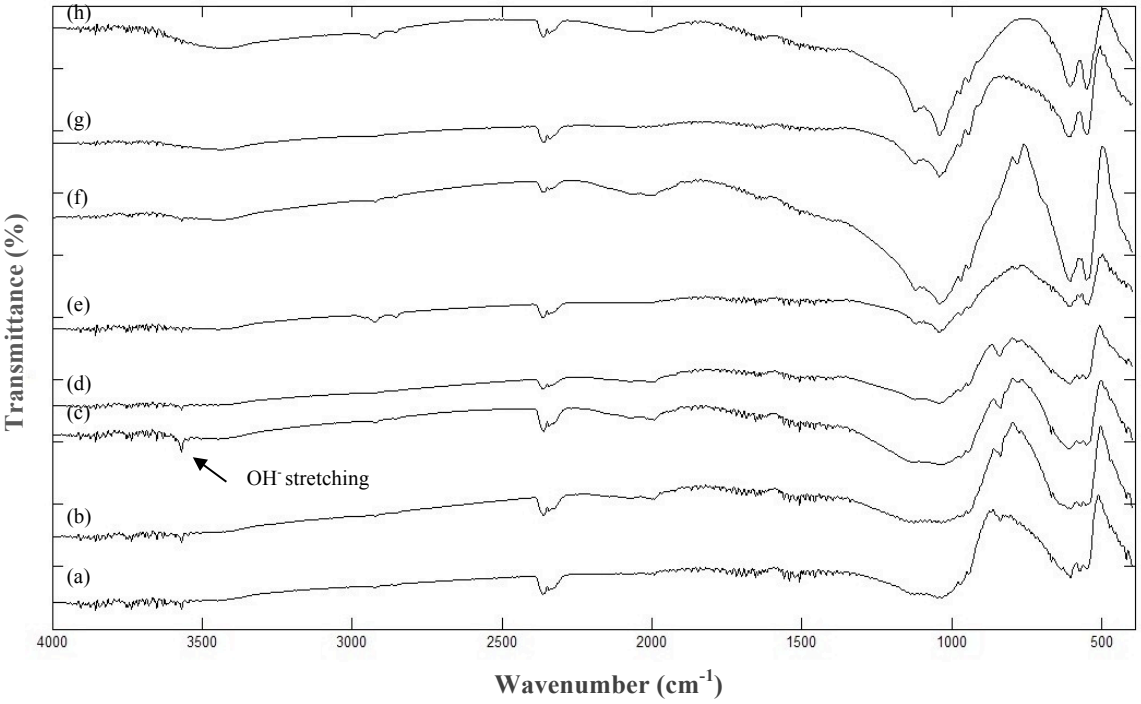

Figure 3.6: FTIR pattern of a) TCP0.5Al (sintered for 1h); b) TCP0.5Al (sintered for 5h); c) TCP1Al (sintered for 1h); d) TCP1Al (sintered for 5h); e) TCP2.5Al (sintered for 1h); f) TCP2.5Al (sintered for 5 h); g) TCP5Al (sintered for 1h); h) TCP5Al (sintered for 5h).

According to Figure 3.7, for the F^- doped samples an increase in the intensity of peaks assigned for OH^- liberation bands were observed by increasing F^- ion content up to 2.5%. While, intensity of peak decreased in TCP5F. It was seen that the hydroxyl band which is located around 3570 cm^{-1} had the lowest intensity in TCP5F, so the intensity of hydroxyl band was decrease by increasing F^- concentration. As a consequence, there is a reduction in the OH^- peak height with increasing F^- ion content. Thus, it can be said the F^- ions substituted for the OH^- groups. These results are in correlation with the investigation of Azami et al. which proved that the intensity of the $\upsilon_4PO_4^{3-}$ (O-P-O) bend at 605cm^{-1} increase, while the $\upsilon_4PO_4^{3-}$ (O-P-O) bend at 565 cm^{-1} is decreased by increasing the degree of fluorination [138].

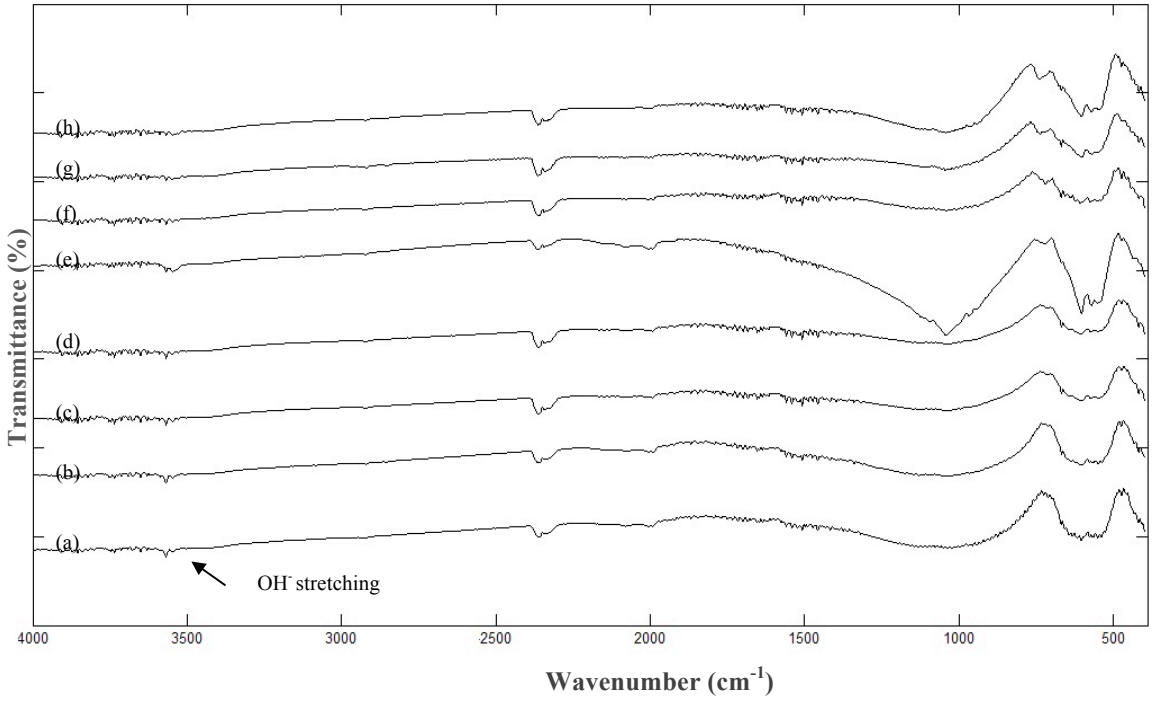

Figure 3.7: FTIR pattern of a) TCP0.5F (sintered for 1h); b) TCP0.5F (sintered for 5h); c) TCP1F (sintered for 1h); d) TCP1F (sintered for 5h); e) TCP2.5F (sintered for 1h); f) TCP2.5F (sintered for 5h); g) TCP5F (sintered for 1h); h) TCP5F (sintered for 5h).

Also, F^- ions incorporated with OH^- ions around the frequency of OH^- stretching bands. It is clearly seen in Figure 3.8, the intensity of peaks around the OH^- stretching band (3570 cm^{-1}) decreased by increasing the amount of F^- and also the peaks are shifted to right (3548 cm^{-1}). These results indicated the incorporation of F^- ions into OH^- ions.

In Figure 3.8, OH^- librational and PO_4^{3-} groups are not visible in FTIR pattern of TCP0.5Al,0.5F. However, OH^- stretching peak is visible around 3600 cm^{-1} but its intensity is too small due to incorporation of the F^- ions in the structure. While the intensity of OH^- stretching was decreased by increasing F^- ion content, the peaks of PO_4^{3-} groups and OH^- librational are visible in other samples.

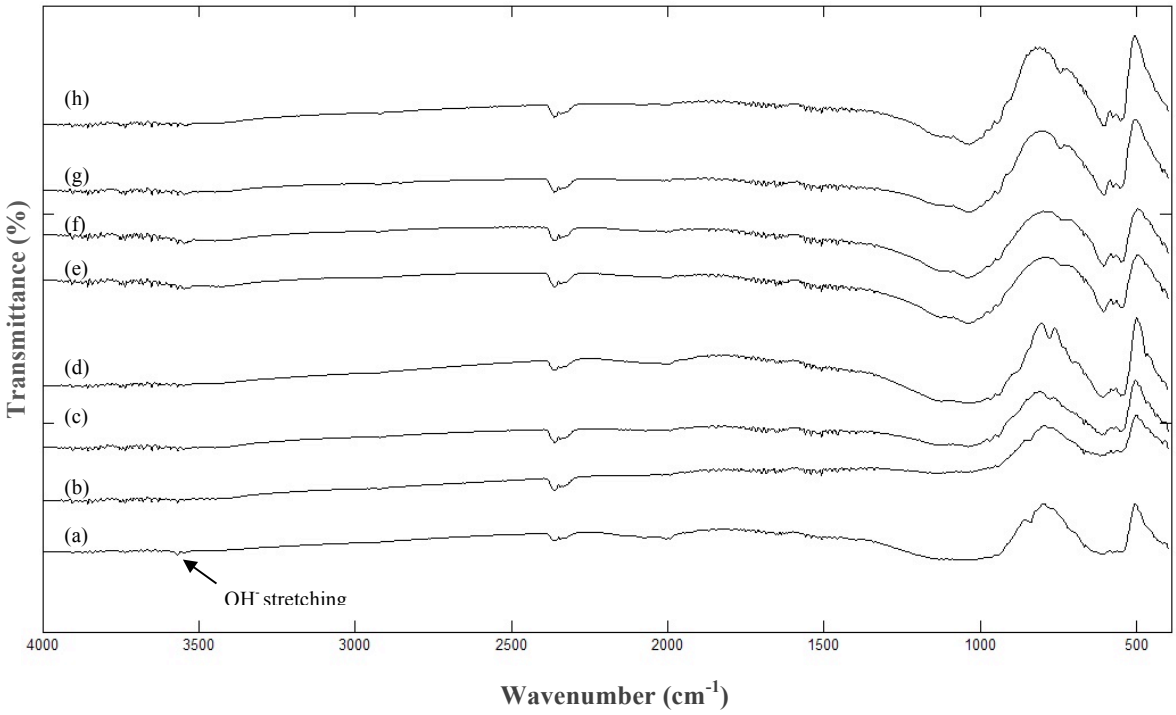

Figure 3.8: FTIR pattern of a) TCP0.5Al,0.5F (sintered for 1h); b) TCP0.5Al,0.5F (sintered for 5h); c) TCP2.5Al,1F (sintered for 1h); d) TCP2.5Al,1F (sintered for 5h); e) TCP2.5Al,2.5F (sintered for 1h); f) TCP2.5Al,2.5F (sintered for 5h); g) TCP2.5Al,5F (sintered for 1h); h) TCP2.5Al,5F (sintered for 5h).

3.2.3 Microstructure of the Samples

SEM images of pure and doped TCPs are presented in Figures 3.9 to 3.12. All of the images were taken from the samples sintered at 1100^{o}C for 1 and 5h. It was seen that the grain size of TCP increased by extending the sintering time (Figure 3.9). Also, both of the samples had dense structures.

It was proved that there is relationship between amount of dopant and temperature with grain sizes of apatites [140]. HAs sintered at low temperatures had more uniform microstructures. However, its grain sizes were exhibited severe increase by increasing of sintering time [140]. They proved that HA has a nano size

grain structure after sintering at 900 and 1100^{o}C, while there is severe grain growth after sintering at 1300^{o}C [140]. According to Figure 3.9, it could be concluded, extending of sintering time has an important effect on grain size of the samples.

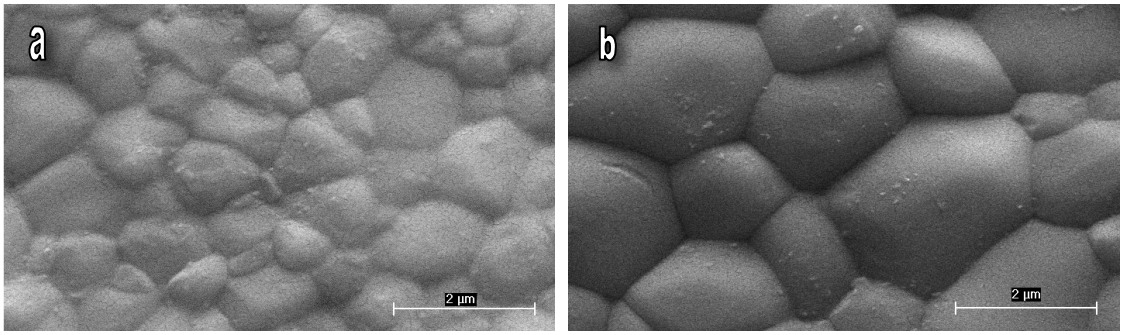

Figure 3.9: SEM images of a) TCP (sintered for 1h); b) TCP (sintered for 5h).

It was clearly observed that the grain size of pure and doped TCPs increased by extending the sintering time for all of the samples. The increase in grain size of β-TCP can be explained by attention to nucleation-aggregation-agglomeration-growth mechanism [68]. This mechanism describes the generation of β-TCP through following steps: (1) generation of β-TCP by nucleation and growth; (2) molecular attraction to aggregation of nanocrystals; (3) further crystal growth [68]. Thus, these increases in grain size of the samples were occurred because nucleus has enough time to grow.

According to Figure 3.10, doping of TCP with Al^{3+} has significant effect on structure and grain size of the samples. So, it can change the mechanical properties of TCP. It was clearly observed that the samples which are doped with Al^{3+} ions have porous structure and this porosity has direct relation with increasing the content of Al^{3+} ions. SEM images showed that porosity of the samples increased by increasing the Al^{3+} ions content. This observation was verified by results of micro-hardness test. Moreover, substitution of Al^{3+} ions into TCP has a significant effect on grain size. According to these images, grain size of the samples were decreased in comparison to pure TCP and this decrease in grain size was increased by

increasing Al^{3+} content. These results are in correlation with investigation of Z. Evis which shows that grain size of HA doped with the Al^{3+} is smaller than that of pure HA [89].

It was reported that the degree of decomposition has a significant effect on morphological structure of the samples [137]. The SEM images show that the porosity of the samples were increased by increasing the Al^{3+} concentration and also according to XRD results, Al^{3+} ions accelerate the decomposition of HA to other phases. As a consequence, an increase in the degree of decomposition negatively affected the densification of the samples.

It was demonstrated, HA decomposes to TCP by the following reaction [141]:

$$Ca_{10}(PO_4)_6(OH)_2 \rightarrow 3Ca_3(PO_4)_2 + CaO + H_2O \quad (3.1)$$

Since one of the products of this reaction is water and water is should going out, pores are generated in the material [141]. It could be concluded that the pores structure of Al^{3+} doped TCPs is because of the reaction related to the decomposition of HA. Since Al^{3+} accelerates decomposition of HA to TCP, increasing Al^{3+} ion content cause an increase in porosity of the samples.

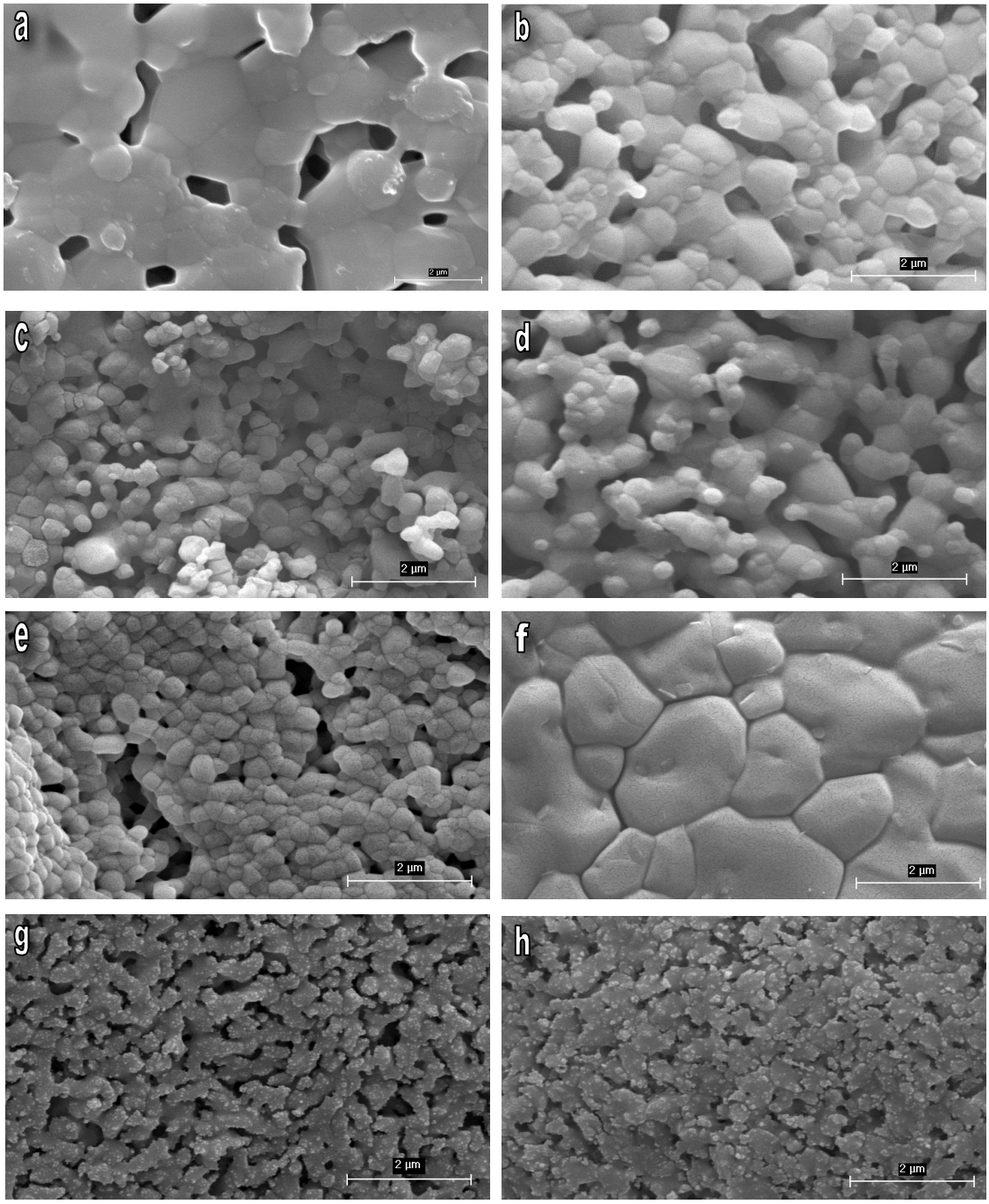

Figure 3.10: SEM images of a) TCP0.5Al (sintered for 1h); b) TCP0.5Al (sintered for 5h); c) TCP1Al (sintered for 1h); (d) TCP1Al (sintered for 5h); e) TCP2.5Al (sintered for 1h); f) TCP2.5Al (sintered for 5h); g) TCP5Al (sintered for 1h); h) TCP5Al (sintered for 5h).

Grain sizes of the samples were increased by increasing the F^- content (Figure 3.11). However, the samples which doped with F^- ions have not a porous structure. This result is in correlation with micro-hardness results which shows that doping of the samples with F^- ions cause an increase in hardness. It was reported that the doping of HA with Y^{3+} and F^- prevented decomposition of HA to TCP and resulted an increase in density [140]. Thus, it could be concluded that F^- ions has a positive effect on density of the samples due to preventing of decomposition of HA.

Samples doped with F^- ions had a dense structure and there was not a pore in the surface of the samples. This phenomenon is proved that F^- ions decrease decomposition rate of HA to β-TCP which is in correlation with the investigation of Kim et al. [137].

It was reported that fluoride had a significant effect on crystal size and stability of apatite structures, F^- ions decreased the crystal size and increase the stability [138]. This phenomenon can be explained by making attention to the crystal structure of apatites which has disorder in their crystal structure. They proved that F^- ions substituted with OH^- groups decrease the degree of disordered in HA structure and theoretically, 50% of F^- ion concentration is enough to stabilize the HA structure by changing the arrangement of F^- ions between OH^- groups [138]. Although, this concentration could be increased in experiments due to the random substitution of OH^- ions with F^- ions [138].

Figure 3.11, shows that the crystal size of our samples decreased by increasing the F^- ion concentration. However, the crystals size of TCP5F sintered 1h shows an increase. This phenomenon could be explained by considering to the amount of F^- ions which is enough to stabilizing the structure of β-TCP.

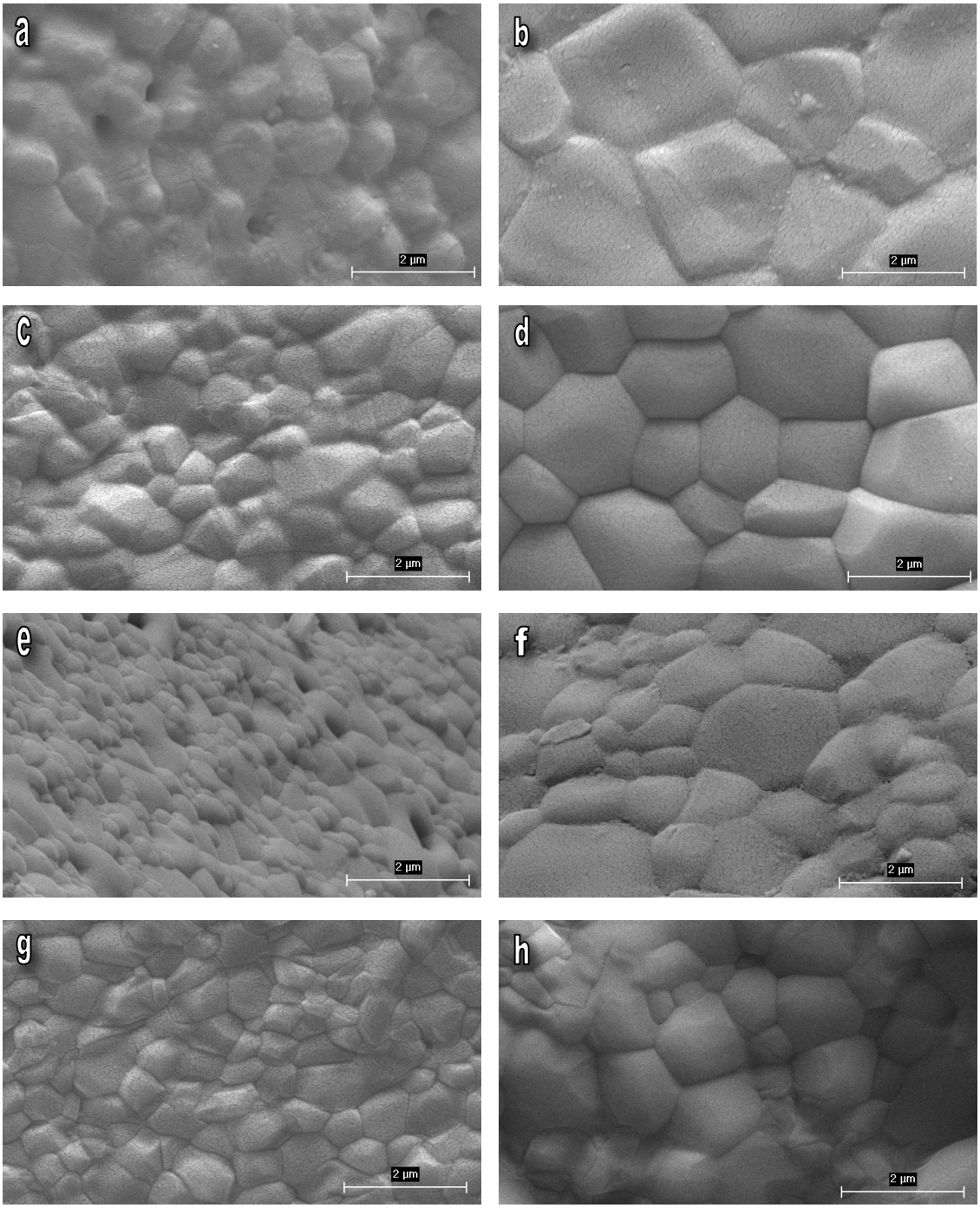

Figure 3.11: SEM images of a) TCP0.5F (sintered for 1h); b) TCP0.5F (sintered for 5h); c) TCP1F (sintered for 1h); d) TCP1F (sintered for 5h); e) TCP2.5F (sintered for 1h); f) TCP2.5FF (sintered for 5h); g) TCP5F (sintered for 1h); h) TCP5F (sintered for 5h).

According to Figure 3.12, the samples doped with Al^{3+} and F^- ions have porous structure and also smaller grain size when compared with pure TCP. As the content of F^- ions increased, grain size of the samples decreased. It was proved that the bond which is formed between OH^- and F^- ions affect the densification rate and grain growth [121].

There are lots of pores throughout the surfaces of the samples which indicate the occurrence of poor densification of the samples doped with Al^{3+} and F^- ions. According to Figure 3.12 (a) and (c) the porosity of the sample increases by increasing the Al^{3+} concentration because Al^{3+} ions accelerate the decomposition of HA. While, the porosity of the samples were decreased by increasing F^- ions content due to decreasing decomposition rate of HA to TCP, so it can be said the degree of decomposition has a significant effect on morphological structure of the samples.

According to Table 3.9, TCP2.5Al had the smallest grain size which is about 180 nm. Also, grain sizes of the samples were increased by extending the sintering time because the nuclei have enough time to nucleation and growth.

In Group 2, the grain size of the samples were decreased by increasing the Al^{3+} concentration and β-TCP wt. fraction of the samples were increased by increasing the Al^{3+} ions content. As a consequence, the purity of the samples could be a factor in reducing the grain size.

In Group 3, the grain size of the samples reduces with increasing the percent of β-TCP. So that, TCP2.5F has the smallest grain size in this group with the highest β-TCP wt. fraction. It was reported that the grain size of F^- doped HA decreased by increasing degree of fluoridation [140].

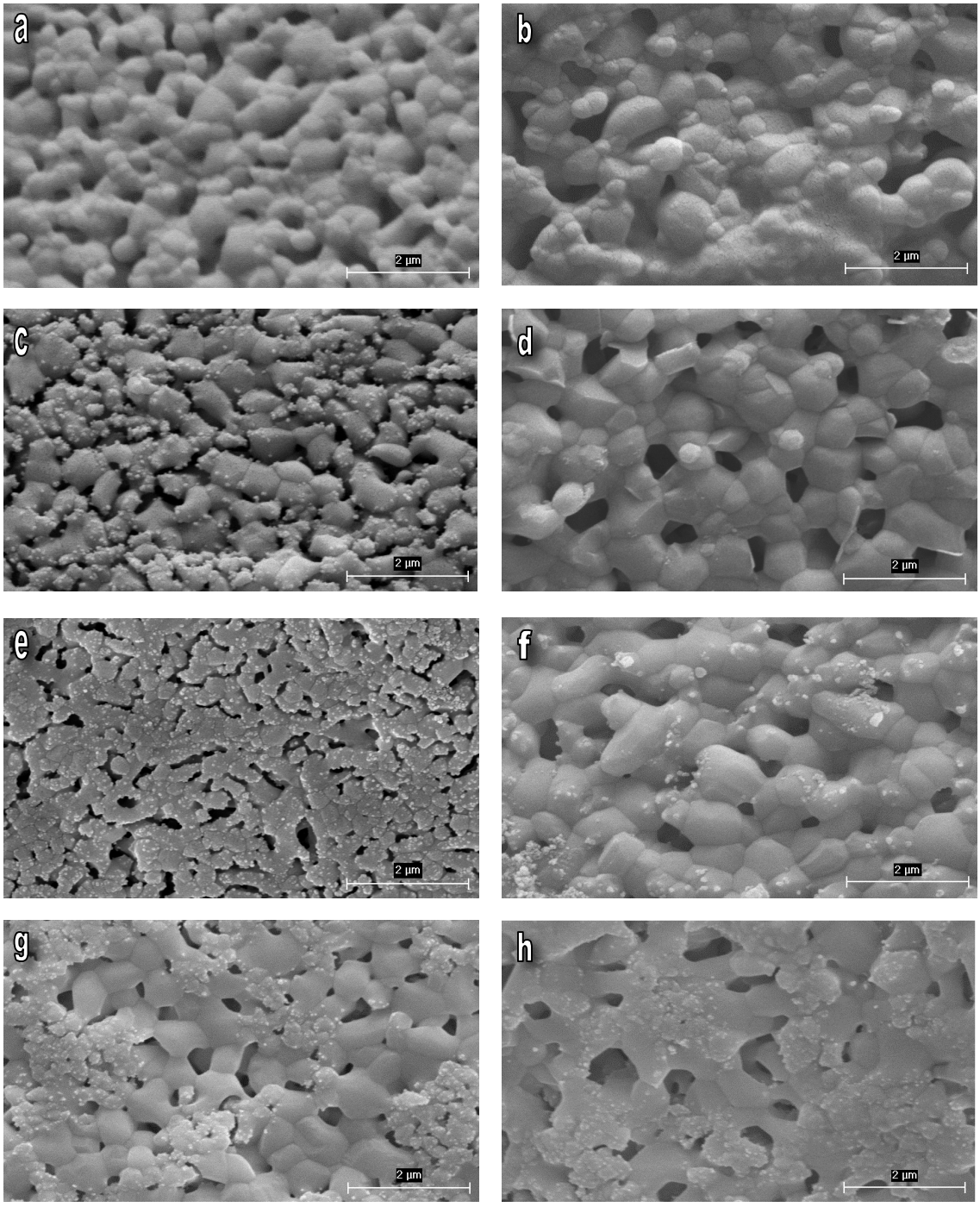

Figure 3.12: SEM images of a) TCP0.5Al,0.5F (sintered for 1h); b) TCP0.5Al,0.5F (sintered for 5h); c) TCP2.5Al,1F (sintered for 1h); d) TCP2.5Al,1F (sintered for 5h); e) TCP2.5Al,2.5F (sintered for 1h); f) TCP2.5Al,2.5FF (sintered for 5h); g) TCP2.5Al,5F (sintered for 1h); h) TCP2.5Al,5F (sintered for 5h).

Table 3.9: Average grain size of pure and doped TCPs sintered at 1100°C for 1 and 5h.

Group No.	Sample ID	Ave. Grain Size (nm) of 1h	Ave. Grain size (nm) of 5h
1	TCP	1305	3055
2	TCP0.5Al	779	948
	TCP1Al	221	398
	TCP2.5Al	180	1027
	TCP5Al	193	238
3	TCP0.5F	849	1000
	TCP1F	724	3055
	TCP2.5F	315	1444
	TCP5F	682	1583
4	TCP0.5Al,0.5F	374	416
	TCP2.5Al,1F	401	849
	TCP2.5Al,2.5F	248	819
	TCP2.5Al,5F	603	861

According to Table 3.9, pure TCP had the largest grain size for all of the sintering times in comparison with doped TCPs. Also, the grain sizes of the same sample increase by extending the sintering time. Thus, this increase in grain size is due to extending of sintering time. Moreover, at the same sintering time, the grain sizes of the samples decrease by increasing the doping ions amount which could be attributed to dopings.

It was reported that HA grains are able to growth on high sintering temperature because the higher temperatures provide the enough activation energy which is necessary for grain growth. Also, they demonstrated that the grain size of HA samples decreased by increasing the amount of doped ions at same sintering temperature [140].

3.3 Mechanical Tests

3.3.1 Vickers Micro-Hardness Tests

Micro-hardness test was performed on samples sintered at 1100°C for 1 and 5 h to investigate the effect of dopant on their mechanical properties. The micro-hardness values of samples are reported in Table 3.10.

Table 3.10: Micro-hardness values of pure and doped TCPs at 1100°C for 1 and 5h.

Group No.	Sample ID	Micro-Hardness (GPa) 1 h	Micro-Hardness (GPa) 5 h
1	TCP	4.71 ± 0.40	4.47 ± 0.28
2	TCP0.5Al	1.17 ± 0.09	1.40 ± 0.11
	TCP1Al	2.80 ± 0.03	2.31 ±0.02
	TCP2.5Al	1.84 ± 0.04	1.47 ± 0.03
	TCP5Al	1.30 ± 0.02	1.09 ± 0.00
3	TCP0.5F	5.73 ± 0.17	4.70 ± 0.33
	TCP1F	5.56 ± 0.15	4.89 ± 0.15
	TCP2.5F	3.33 ± 0.13	2.90 ± 0.19
	TCP5F	3.46 ± 0.33	2.89 ± 0.12
4	TCP0.5Al,0.5F	1.41 ± 0.09	1.34 ± 0.10
	TCP2.5Al,1F	0.37 ± 0.03	0.37 ± 0.03
	TCP2.5Al,2.5F	0.49 ± 0.05	0.40 ± 0.04
	TCP2.5Al,5F	0.44 ± 0.01	0.42 ± 0.01

According to Table 3.10, micro-hardness values of the samples were decreased by extending the sintering time of the samples. While TCP0.5Al showed an increase in micro hardness after extending the sintering time, it is possible to say that increasing the sintering time negatively affected the mechanical properties of all of the samples. This phenomenon can be explained by considering the increase in grain size after extending the sintering time.

It was reported that the hardness of HA and FHA was increased by increasing sintering temperature but a decrease was observed with increasing degree

of fluoridation [134]. Indeed the hardness of samples with higher degree of fluoridation exhibit a decrease by increasing of sintering temperature [134].

It was reported that an increase in hardness is related with the reduction in the porosity, which is known as the Duckworth-knudsen exponential model [137]. As seen in Table 3.10, samples doped with Al^{3+} ions show a great decrease in micro-hardness due to their highly porous structure. While, the samples doped with F^- ions have high micro-hardness values.

TCP0.5F sintered at 1100^oC for 1 h had the highest micro-hardness value when compared with other samples but increasing the amount of F^- ions cause a decrease in micro-hardness values. These results exhibited a consistency with investigation, which proved that incorporation of F^- ions improved mechanical property just up to a certain limit [134]. It was reported that the partial substitution of OH^- ions by F^- ions causes an improvement in mechanical properties and proved that during partial substitution of OH^- by F^- ions, hydrogen ions which are participated in OH^- bound with F^- instead of O^{2-} ions, so produced a good ordered apatite structure which improved mechanical properties [135].

In Group 4, TCP0.5Al,0.5F has the highest micro-hardness, while TCP2.5Al,1F shows the smallest micro-hardness. However, there was a little increase in micro-hardness of the samples with increasing F^- concentration which shows that F^- ions improved mechanical properties of calcium phosphates. Also, it is proved that morphological structure has a considerable effect on mechanical properties, so that among the samples of Group 4, TCP0.5Al,0.5F has higher density.

According to Figure 3.13, the hardness of pure TCP has a tendency to decrease with increasing the relative density while it was reported that the hardness of HA decreased due to a decline in density [134]. Also, it is possible to say that TCP0.5Al and TCP1Al has a tendency to exhibit a decrease in the hardness by increasing the density of the samples. However, the hardness of TCP2.5Al and TCP5Al is increased with increasing the density.

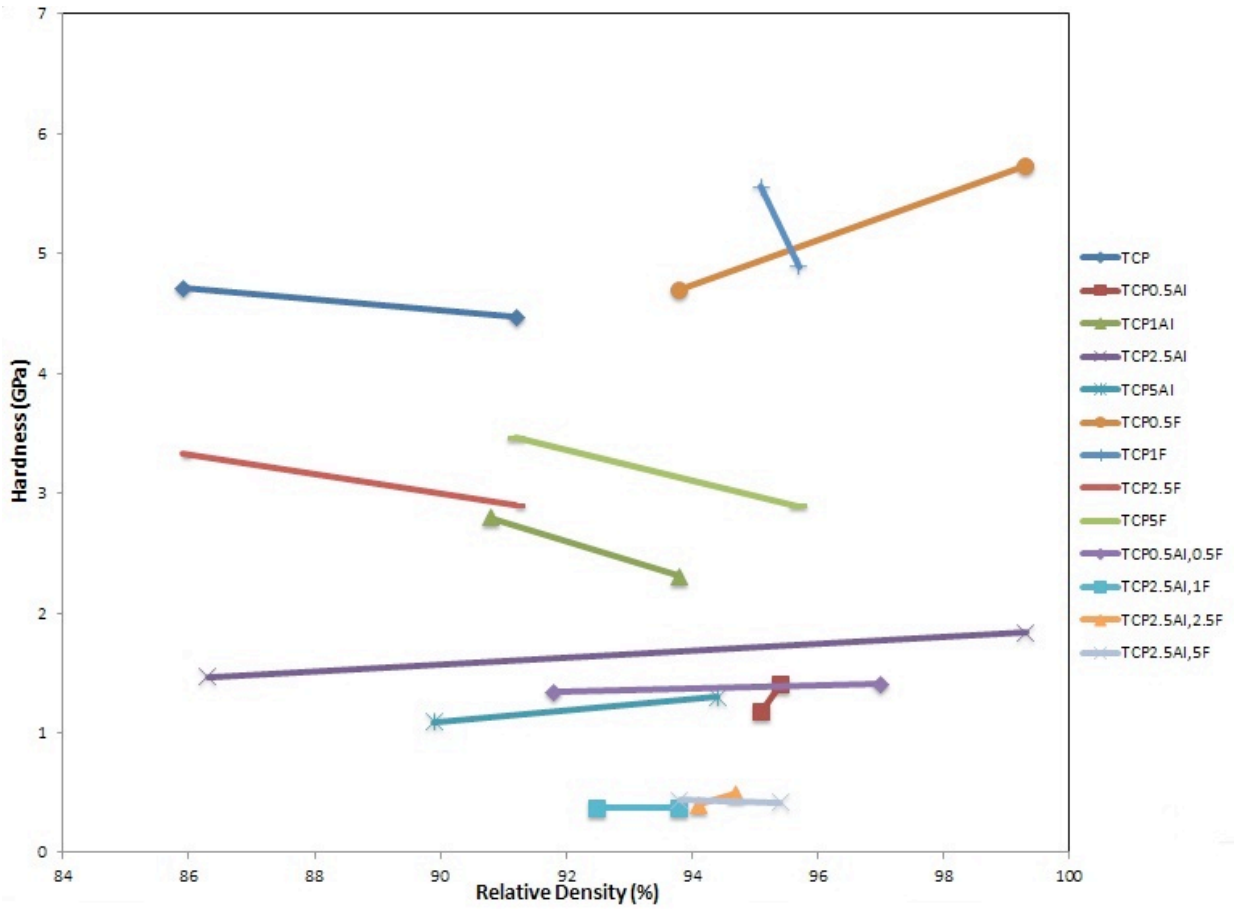

Figure 3.13: The effect of density on hardness of the materials.

The tendency occurred to decrease of hardness with increasing of density for all of the fluoride doped samples except for TCP0.5F. The hardness of TCP0.5F exhibits a significant increase with an increase in relative density. While, it was reported that the hardness of hydroxyfluorapatite has tendency to increase with an increase in density [134].

It was proved that hardness has a linear relationship with pore content [134]. Also, it was reported higher density has an important role in producing higher hardness values when an increase in density and grain size cause an increase in hardness [134].

3.3.2 Diametral Tensile Strength

Diametral tensile strength is highly recommended for biomaterials, for example, teeth prosthesis biomaterials and also cement utilize in the dentistry [120]. There is great similarity between the stresses formed in implants which used in dentistry and stresses which formed during diametral tensile strength test [142].

Previous studies showed that tensile strength values depend on different factors such as porosity, contact area, diameter, thickness, poisson ratio, grain size and distribution of the pores in the samples [142,143]. It was reported that increasing of relative density has a positive effect of diametral tensile strength of HA, indeed there is an increase in tensile strength of HA by increasing the relative density of the samples [144]. Also, presence of second phase has a considerable effect on tensile strength values. Theoretical tensile strength that was reported for completely dense HA is around 35 MPa while for HA which has open pore structure; this value is around 1-2 MPa [145]. This Varity in diametral tensile strength values shows that different factors have great effect on test results.

Table 3.11 exhibits the diametral tensile strength test results. According to this table, there is a decrease in tensile strength values by extending sintering time in all of the groups. This suggests that increasing the grain size has negative effect on mechanical properties of the samples.

In the samples of Group 1, there is an increase in the relative density of the samples. However, it was shown a considerable decrease by extending the sintering time. This suggest that other factors such as grain size and the percent of second phase negatively affected the tensile strength of the sample by extending the sintering time. This result is in correlation with grain size of the samples of Group 1, which shows in Table 3.8, so a decrease in grain size enhance the mechanical properties of TCP.

Table 3.11: Diametral tensile strength values of pure and doped TCPs at 1100°C for 1 and 5 h.

Group No.	Sample ID	Tensile Strength (MPa) 1 h	Tensile Strength (MPa) 5 h
1	TCP	3.82 ± 1.73	1.03 ± 2.85
2	TCP0.5Al	4.01 ± 1.80	3.74± 1.68
	TCP1Al	6.08 ± 2.03	5.53 ±1.42
	TCP2.5Al	7.01 ± 3.24	5.85 ± 2.50
	TCP5Al	8.11 ± 2.19	6.83 ± 3.15
3	TCP0.5F	15.65 ± 2.87	13.70 ± 1.24
	TCP1F	18.10 ± 3.09	12.60 ± 1.51
	TCP2.5F	20.83 ± 2.19	12.98 ± 3.15
	TCP5F	12.45 ± 4.26	10.41 ± 1.89
4	TCP0.5Al,0.5F	8.50 ± 2.69	7.62 ± 1.68
	TCP2.5Al,1F	7.04 ± 4.81	4.27 ± 1.60
	TCP2.5Al,2.5F	9.81 ± 2.83	6.38 ± 3.80
	TCP2.5Al,5F	8.01 ± 1.92	5.42 ± 2.01

Presence of second phases could lead to a decrease in the mechanical properties bioceramics. For example, it was proved that presences of β-TCP and HA as a second phase decline the mechanical properties of biphasic biomaterials [146]. This phenomena is due to existence of the stress between the different phases because of the difference in the thermal expansion coefficient of two different phases [147]. However, the biphasic ceramics widely utilized as biomaterials due to their good biological reactivity and bonding with bone in comparison with pure ceramics [147,148]. Also, it was reported that β-TCP improve the mechanical properties of the samples because of its high rate of dissolution, which promote bone in-growth [147,148].

In Group 2, there is a correlation among the tensile strength values and relative densities of the samples except for TCP5Al and TCP1Al. According to the results of this group, TCP2.5Al had the highest relative density and the smallest grain size while TCP5Al had the highest tensile strength value. This phenomenon might be explained by considering the influence of second phase on mechanical

properties of the samples. According to the Rietveld analysis results, increasing the Al^{3+} ion content declined wt. fraction of HA. Thus, TCP5Al is not a biphasic material and there are no stresses between different phases, which cause a decline in mechanical properties.

According to results in Group 3 of Table 3.11, TCP2.5F has the highest diametral tensile strength value among the samples while TCP0.5F has the highest relative density. However, the grain size of the grain size of the TCP2.5F is considerably smaller than other samples of this group. Also, the diametral tensile strength of the samples that doped with F^- ions is greater than other groups. This phenomenon might be explained by considering to SEM results, which show that these samples have a dense structure and there are no lots of pore in the structure of the samples, which cause decline mechanical properties of materials. These results suggested that doping of calcium phosphates with F^- improve mechanical properties of calcium phosphates.

Among the samples of Group 4, TCP2.5Al,2.5F has the highest tensile strength value and the smallest grain size. There is a correlation between grain size and diametral tensile strength values in this group. Also, doping with Al^{3+} and F^- ions improve mechanical properties in comparison with pure TCP.

CHAPTER 4

4. CONCLUSION

In this study, TCP was synthesized by a precipitation method and doped with various amounts of Al^{3+} and/or F^- ions in order to investigate its microstructural and mechanical properties. All of the samples were sintered at 1100 ^oC for 1 and 5h.

Density of the samples doped with Al^{3+} showed a considerable increase. However, density of the samples decreased by extending the sintering time except for TCP1Al and TCP0.5Al. Doping of TCP with F^- ions resulted a decrease in density of the samples. In the samples doped with F^- ions, densification increased by extending the sintering time except for TCP0.5F.

The structural analysis determined by Rietveld refinement proved the presence of β-TCP as the main phase. Presence of these phases is essential due to dopants and synthesis method. The HA phase was detected besides β-TCP, resulting in the formation of HA/β-TCP biphasic composites with different compositions. Lattice parameters decreased upon ions substitution.

Scanning electron microscopy (SEM) results showed that addition of doping ions resulted in smaller grains. In Fourier transform infrared spectroscopy (FTIR), in addition to the characteristic bands of TCP, F^- ion substitution was confirmed. In general, the micro hardness test revealed that Al^{3+} ions in large amounts had negative effects on the mechanical properties of the samples, while substitution of the F^- ions improved the mechanical properties of the samples.

REFERENCES

[1] R.Z. Legeros, “Biological and Synthetic Apatites”, Editors: P.W. Brown, B. Constantz , Hydroxyapatite and Related Materials, CRC Press, Boca Raton, USA (1994) 3-28.

[2] M. Yoshimura, H. Suda, “Hydrothermal processing of hydroxyapatite: Past, present and future”, Editors: P.W. Brown, B. Constantz, Hydroxyapatite and Related Materials, CRC Press, Boca Raton, USA (1994) 45-72.

[3] J.A. Weatherell, C. Robinson, “The inorganic composition of teeth”; in Zipkin I. (ed): Biological Mineralization, John Wiley, NY, USA (1973) 43-74.

[4] M.J. Dallemagne, L.J. Richelle, “Inorganic chemistry of bone”; in Zipkin I. (ed): Biological Mineralization, John Wiley, NY, USA (1973) 23-42.

[5] Q. Song, C. Wang, S. Wen, “Effects of doping on crystal and grain boundary in human enamel”, Materials Science and Engineering A 297 (2001) 272-280.

[6] A. Krajewski, A. Ravaglioli, S. Wen, J.W. Feng, “Microstructural features of synthetic ceramized chlorapatite in comparison with human enamel crystals”, Journal of Applied Crystallography 25 (1992) 465-470.

[7] C. Frondel, “Mineralogy of the calcium phosphates in insular phosphate rock”, American Mineralogist 28 (1943) 215-232.

[8] D. McConnell, “Apatite, its crystal chemistry, mineralogy, utilization, and geologic and biologic occurrences”, Materials Science Monograph 51 (1989) 221-228.

[9] J.R. Lehr, E.H. Brown, A.W. Frazier, “Crystallographic properties of fertilizer compounds”, Chemical Engineering Bulletin 6 (1976) 114-132.

[10] J.R. Van Wazer, “Phosphorous and its compounds”, Interscience Publishers, NY, USA (1958) 113-122.

[11] B. Dickens, J.S. Bowen, “Refinement of the crystal structure of $Ca(H_2PO_4)_2 \cdot H_2O$”, Acta Crystallographica B27 (1971) 2247-2255.

[12] N. Bjerrum, “Calciumorthophosphate”, Matematisk-fysiske Meddelesler 31 (1958) 1-79.

[13] M. Mathew, W.E. Brown, L.W. Schroder, “Crystal structure of octacalcium bis (hydrogenphosphate) tetrakis (phosphate) pentahydrous”, Crystal Spectroscopy 18 (1988) 1048-1050.

[14] H. El Briak-Benabdesalem, C. Mochales, M.P. Ginebra, J. Nurit, J.A. Pllanel, P. Budeville, “Dry mechanochemical synthesis of hydroxyapatite from dicalcium phosphate dihydrate and calcium oxide: A kinetic study”, Journal of Biomedical Materials Research Part A 67(3) (2003) 927-937.

[15] H. Lizhi, F. Zude, “Preparation and characterization of dicalcium phosphate dihydrate coating on enamel”, Materials Letters 67 (2007) 3923-3926.

[16] C.A. Beevers, “The crystal structure of dicalcium phosphate dehydrate, $CaHPO_4.2\ H_2O$”, Acta Crystalographica 11 (1958) 273-277.

[17] G. Lenart, G. Bildo, J. Pinter, “Some basic problems in the examination of the calcium phophates of bone”, Clinical Orthopedic and Related Research 83 (1972) 263-272.

[18] F. Casciani, R.A. Condrate, “The vibrational spectra of brushite, $CaHPO_4.2\ H_2O$”, Spectroscopy Letters 12 (1979) 699-713.

[19] B. Dickens, J.S. Bowen, W.E. Brown, “A refinement of the crystal structure of $CaHPO_4$ (synthetic monetite)”, Acta Crystalographica B28 (1972) 797-806.

[20] A. Tovboro Jensen, S.L. Rowles, “Magnesian whitlockite, a major constituent of human dental calculus”, Acta Odontologica Scandinavica 15 (1957) 121-139.

[21] M. Mathew, L.W. Schroder, B. Dickens, W.E. Brown, “The crystal structure of α-$Ca_3(PO_4)_2$”, Acta Crystalographica B33 (1977) 1325-1333.

[22] B. Dickens, L.W. Schroder, W.E. Brown, “Crystallographic studies of the role of Mg as a stabilizing impurity in β-$Ca_3(PO_4)_2$, the crystal structure of pure β-$Ca_3(PO_4)_2$”, Journal of Solid State Chemistry 10 (1974) 232-248.

[23] B. Dickens, W.E. Brown, G.J. Kruger, J.M. Stewart, “$Ca_4(PO_4)_2O$, tetracalcium diphosphate monoxide, crystal structure and relationships to $Ca_5(PO_4)_3OH$ and $K_3Na(SO_4)_2$”, Acta Crystalographica B29 (1973) 2046-2056.

[24] B.K. Hall, “Bone matrix and bone specific products”, Bone, CRC Press, Boca Raton, USA Vol. 1 (1991) 55-70.

[25] J.B. Lian, G.S. Stein, E. Canalis, P. Gehron-Robey, A.L. Boskey, “Bone formation: Osteoblast lineage cells, growth factors, matrix proteins and the

mineralization process", Prime on the metabolic bone disease and disorders of mineral metabolism, Fourth edition, Academic Press, NY, USA (1999) 14-29.

[26] P. Gehron-Robey, A.L. Boskey, "The biochemistry of bone", Osteoporosis: Etiology, Diagnosis and Management, Academic Press, London, UK (1996) 90-120.
[27] R.B. Martin, D.B. Burr, N.A. Sharkey, "Skeletal Tissue Mechanics", Springer, NY, USA (1998) 29-80.

[28] M.B. Schaffler, D.B. Burr, "Stiffness of compact bone: Effect of porosity and density", Journal of Biomechanics 21 (1988) 13-16.

[29] W.S.S. Jee, "Structure and function of bone tissue, in orthopedics, principles of basic and clinical science", CRC Press, Boca Raton, USA (1999) 112-238.

[30] L. Weiss, "Cell and tissue biology, A text book of histology", CRC Press, Boca Raton, USA (1988) 80-120.

[31] R.B. Martin, D.B. Burr, "Structure, function, and adaptation of compact bone", Raven Press, NY, USA (1989) 34-230.

[32] E.F. Ericksen, D.W. Axelord, F. Melsen, "Bone histomorphology", Bone Histomorphometry, Raven Press, New York, USA (1994) 145-170.

[33] R.B. Ashman, "Experimental techniques in bone mechanics", Edited by S. C. Cowin, CRC Press, Boca Raton, USA (1989) 75-95.

[34] H.A. Yuehui, A.D. Robert, "Mechanical testing of bone and the bone-implant interface", CRC Press, Boca Raton, USA (2000) 41-56.

[35] D.M. Cullinane, T.A. Einhorn, "Biomechanics of Bone" Principles of Bone Biology, Second Edition, Vol. 1, Academic Press, London, UK (2002) 17–32.

[36] N. Sasaki, N. Matsushima, T. Ikawa, H. Yamamura, A. Fukuda, "Orientation of bone mineral and its role in the anisotropic mechanical properties of bone-transverse anisotropy", Journal of Biomechanics 22 (1989) 157-164.

[37] R.B. Martin, D.L. Boardman, "The effect of collagen fiber orientation, porosity, density and mineralization of bovine cortical bone bending properties", Journal of Biomechanics 26 (1993) 1047-1054.

[38] W.J. Whitehouse, "The quantitative morphology of anisotropic trabecular bone", Journal of Microscopy 101 (1974) 153-168.

[39] R. Lazenby, “Porosity-geometry interaction in the conversation of bone strength”, Journal of Biomechanics 19 (1986) 257-258.

[40] D.T. Reilly, A.H. Burstein, “The elastic and ultimate properties of compact bone tissue”, Journal of Biomechanics 8 (1975) 393-397.

[41] J.Y. Rho, R.B. Ashman, C.H. Turner, “Young’s modulus of trabecular and cortical bone material: Ultrasonic and microtensile measurements”, Journal of Biomechanics 26 (1993) 111-119.

[42] J.D. Currey, “Bones structures and mechanics”, CRC Press, Boca Raton, USA (2002) 11-15.

[43] S.M. Besta, A.E. Porter, E.S. Thian, J. Huang, “Bioceramics: Past, present and for the future”, Journal of the European Ceramic Society 28 (2008) 1319–1327.

[44] W.G. Goodman, M.E. Duarte, “Aluminum: Effects on bone and role in the pathogenesis of renal osteodystrophy”, Mineral and Electrolyte Metabolism 17 (1991) 221-232.

[45] J.H. Beattie, H.S. Peace, “The influence of a low-boron diet and boron supplementation on bone, major mineral and sex steroid metabolism in postmenopausal women”, The British Journal of Nutrition 69 (1993) 871-874.

[46] Y. Hojima, B. Behta, A.M. Romanic, D.J. Prockop, “Cadmium ions inhibit procollagen C-proteinase and cupric ions inhibit procollagen N-proteinase”, Journal of International Society for Matrix Biology 14 (1994) 113-120.

[47] T. Miyahara, H. Yamada, M. Takeuchi, H. Kozuka, T. Kato, H. Sudo, “Inhibitory effects of cadmium on in vitro calcification of a clonal osteogenic cell”, Toxicology and Applied Pharmacology 96 (1988) 52-59.

[48] A. Bigi, G. Falini, E. Foresti, M. Gazzano, A. Ripamonti, N. Roveri, “Magnesium influence on hydroxyapatite crystallization”, Journal of Inorganic Biochemistry 49 (1993) 69-78.

[49] R.Z. LeGeros, “Calcium phosphates in oral biology and medicine”, In Monographs in Oral Science, ed. K.H. Myers, Vol. 15, AG Publishers, Basel, Switzerland (1991) 82-107.

[50] S.G. Dahl, P. Allain, P.J. Marie, Y. Mauras, G. Boivin, P. Ammann, Y. Tsoderous, P.D. Delmas, C. Christiansen, “Incorporation and distribution of strontium in bone”, Bone 28 (2010) 446-453.

[51] E.J. O'Flaherty, "Modeling bone mineral metabolism, with special reference to calcium and lead", Neurotoxicology 13 (1992) 789-797.

[52] M. Mousny, S. Omelon, L. Wise, E.T. Everett, M. Dumitriu, D.P. Holmyrad, X. Banse, J.P. Devogealer, M.D. Grynpas, "Fluoride effects on bone formation and mineralization are influenced by genetics", Bone 43 (2008) 1067-1074.

[53] T. Wang, J.C. Zhang, Y. Chen, P.G. Xiao, M.S. Yang, "Effect of zinc ion on the osteogenic and adipogenic differentiation of mouse primary bone marrow stromal cells and the adipocytic trans-differentiation of mouse primary osteoblasts", Journal of Trace Elements in Medicine and Biology: Organ of the Society for Minerals and Trace Elements 21 (2007) 84-91.

[54] E.Jallot, J.M. Nedelec, A.S. Grimault, E. Chassot, "STEM and EDXS characterization of physic-chemical reaction at the periphery of sol-gel derived Zn-substitutes hydroxyapatites during interaction with biological fluids", Colloids and Surfaces B: Biointerfaces 42 (2005) 205-210.

[55] P. Van Landuyt, F. Li, J.P. Keustermans, J.M. Streydio, F. Delannay, E. Munting, "The influence of high sintering temperatures on the mechanical properties of hydroxyapatite", Journal of Materials Science: Materials in Medicine 6 (1995) 8-13.

[56] S.J. Kalita, A. Bhardwaj, H.A. Bhatt, "Nanocrystalline calcium phosphate ceramics in biomedical engineering", Materials Science and Engineering C 27 (2007) 441-449.

[57] J.L. Xu, K.A. Khor, Z.L. Dong, Y.W. Gu, R. Kumar, P. Cheang, "Preparation and characterization of nano-sized hydroxyapatite powders produced in a radio frequency (rf) thermal plasma", Materials Science and Engineering A 374 (2004) 101-108.

[58] M. Itokazu, W. Yang, T. Aoki, A. Ohara, N. Kato, "Synthesis of antibiotic-loaded interporous hydroxyapatite blocks by vacuum method and in vitro drug release testing", Biomaterials 19 (1998) 817-819.

[59] Z. Evis, R.H. Doremus, "Coatings of hydroxyapatite-nanosize alpha alumina composites on Ti-6Al-4V", Materials Letters 59 (2005) 3824-3827.

[60] R.Z. Legeros, J.P. Legeros, In: L.L. Hench, J. Wilson, editors, "An Introduction to Bioceramics", World Scientific Publishing Company, Singapore (1993) 139-180.

[61] S.A. Guechler, J.O. Holinger, “An Introduction to Biomaterials”, CRC Press, Boca Raton, USA (2006) 311-339.

[62] Q. Song, C. Wang, S. Wen, “Effects of doping on crystal and grain boundary in human enamel”, Materials Science and Engineering A 297 (2001) 272-280.

[63] S. Pramanik, A.K. Agarwal, K.N. Rai, A. Garg, “Development of high strength hydroxyapatite by solid-state-sintering process”, Ceramics International 33 (2007) 419–426.

[64] S.-H. Rhee, “Synthesis of hydroxyapatite via mechanochemical treatment”, Biomaterials 23 (2002) 1147–1152.

[65] W.J. Shih, Y.H. Chen, M.C. Wang, M.H. Hon, “Crystal growth and morphology of the nano-sized hydroxyapatite powders synthesized from $CaHPO_4 \cdot 2H_2O$ and $CaCO_3$ by hydrolysis method” Journal of Crystal Growth 270 (2004) 211–218.

[66] I. Mobasherpour, M.S. Heshajin, A. Kazemzadeh, M. Zakeri, “Synthesis of nanocrystalline hydroxyapatite by using precipitation method”, Journal of Alloys and Compounds 430 (2007) 330-333.

[67] W. Feng, L. Mu-sen, L. Yu-peng, Q. Yong-xin, “A simple sol–gel technique for preparing hydroxyapatite nanopowders”, Materials Letters 59 (2005) 916– 919.

[68] K.P. Sanosh, M.C. Chu, A. Balakrishnan, T.N. Kim, S.J. Cho, “Sol-gel synthesis of pure nanosize β-tricalcium phosphate crystalline powders”, Current Applied Physics 10 (2010) 68-71.

[69] J.S. Chen, H.Y. Juang, M.H. Hon, “Calcium phosphate coating on titanium substrate by a modified electrocrystallization process”, Journal of Materials Science: Materials in Medicine 9 (1998) 297-300.

[70] S. Ramesh, C.Y. Tan, I. Sopyan, M. Hamdi, W.D. Teng, “Consolidation of nanocrystalline hydroxyapatite powder”, Science and Technology of Advanced Materials 8 (2007) 124-130.

[71] M.A. Meyers, P.Y. Chen, A.Y.M. Lin, Y. Seki, “Biological materials: Structure and mechanical properties”, Progress in Materials Science 53 (2008) 1-206.

[72] C.H. Turner, J. Rho, Y. Takano, T.Y. Tsui, G.M. Pharr, “The elastic properties of trabecular and cortical bone tissues are similar: Results from two microscopic measurement techniques”, Journal of Biomechanics 32 (1999) 437-441.

[73] L.-H. He, O.C. Standard, T.T.Y. Huang, B.A. Latella, M.V. Swain, "Mechanical behavior of porous hydroxyapatite", Acta Biomaterialia 4 (2008) 577-586.

[74] J.J. Klawitter, S.F. Hulbert, "Application of porous ceramics for the attachment of load bearing internal orthopedic applications", Journal of Biomedical Materials Research 5 (1971) 161-229.

[75] R.A. Ayers, L.M. Wolford, T.A. Bateman, V.L. Ferguson, S.J. Simske, "Qualification of bone ingrowth into porous block hydroxyapatite in humans", Journal of Biomedical Materials Research 47 (1999) 54-59.
[76] T. Kokubo, "Bioceramics and their clinical applications", CRC Press, Boca Raton, USA (2008) 92-353.

[77] H. Denissen, C. Mangano, G. Venini, "Hydroxyapatite implants", Piccin Nuova Libraria, Spa: Padua (1985) 160-170.

[78] T.J. Webster, E.A. Massa-Schlueter, J.L. Smith, E.B. Slamovich, "Osteoblast response to hydroxyapatite doped with divalent and trivalent cations", Biomaterials 25 (2004) 2111–2121.

[79] Z.Y. Li, W.M. Lam, C. Yang, B. Xu, G.X. Ni, S.A. Abbah, K.M.C. Cheung, K.D.K. Luk, W.W. Lu, "Chemical composition, crystal size and lattice structural changes after incorporation of strontium into biomimetic apatite", Biomaterials 28 (2007) 1452–1460.

[80] M.E. Fleet, X. Liu, Y. Pan, "Site preference of rare earth elements in hydroxyapatite [$Ca_{10}(PO_4)_6(OH)_2$]", Journal of Solid State Chemistry 149 (2000) 391-398.

[81] L.L. Hench, J. Wilson, "**An Introduction to Bioceramics", World Scientific Vol. 1, NJ, USA (1993) 139-180.**

[82] Q. Song, C. Wang, S. Wen, "Effects of doping on crystal and grain boundary in human enamel", Materials Science and Engineering A 297 (2001) 272-280.

[83] C. Ergun, T.J. Webster, R. Bizios, R.H. Doremus, "Hydroxylapatite with substituted magnesium, zinc, cadmium, and yttrium. I. Structure and microstructure", Journal of Biomedical Materials Research Part A 59 (2001) 305–311.

[84] T.J. Webster, C.Ergun, R.H. Doremus, R. Bizios, “Hydroxylapatite with substituted magnesium, zinc, cadmium, and yttrium. II. Mechanisms of osteoblast adhesion”, Journal of Biomedical Materials Research Part A 59 (2002) 312-317.

[85] X. Cao, W. Harris, “Carbonate and magnesium interactive effect on calcium phosphate precipitation”, Environmental Science & Technology 42 (2008) 436-442.

[86] H.S. Ryu, K.S. Hong, J.K. Lee, D.J. Kim, J.H. Lee, B.D. Chang, D. Lee, C.K. Lee, S.S. Chung, “Magnesia-doped HA/β-TCP ceramics and evaluation of their biocompatibility”, Biomaterials 25 (2004) 393-401.

[87] S. Kannan, J.M. Ventura, J.M.F. Ferreira, “Aqueous precipitation method for the formation of Mg-stabilized β-tricalcium phosphate: An x-ray diffraction study”, Ceramics International 33 (2007) 637-641.

[88] J. Tian, S. Zhang, Y. Shao, H. Shan, “Nanosize SiC particle reinforced hydroxyapatite composites”, In: Proceedings of the Bioceramics: Materials and Applications II Symposium (1995) 107-114.

[89] Z. Evis, “Al^{3+} doped nano-hydroxyapatites and their sintering characteristics”, Journal of the Ceramic Society of Japan 114 (2006) 1001-1004.

[90] A. Machoy-Mokrzynska, “Fluoride- magnesium interaction”, Journal of the International Society for Fluoride Research 28 (1995) 175-177.

[91] H. Eslami, M. Solati-Hashjin, M. Tahriri, “The comparison of powder characteristics and physicochemical, mechanical and biological properties between nanostructure ceramics of hydroxyapatite and fluoridated hydroxyapatite”, Materials Science and Engineering C 29 (2009) 1387-1398.

[92] H. Qu, M. Wei, “The effect of fluoride contents in fluoridated hydroxyapatite on osteoblast behavior”, Acta Biomaterialia 2 (2006) 113–119.

[93] E. Fernândez, F.J. Gil, M.P. Ginebra, F.C.M. Driessens, J.A. Planell, S.M. Best, “Calcium phosphate bone cements for clinical applications. Part I: Solution chemistry”, Journal of Materials Science: Materials in Medicine 10 (1999) 169-176.

[94] S.J. Kalita, A. Bhardwaj, H.A. Bhatt, “Nanocrystalline calcium phosphate ceramics in biomedical engineering”, Materials Science and Engineering C 27 (2007) 441–449.

[95] T. Landete-Castillejos, J.D. Currey, J.A. Estevez, E. Gaspar-López, A. Garcia, L. Gallego, “Influence of physiological effort of growth and chemical composition on antler bone mechanical properties”, Bone 41 (2007) 794–803.

[96] S. Ni, J. Chang, “In vitro degradation, bioactivity, and cytocompatibility of calcium silicate, dimagnesium silicate, and tricalcium phosphate bioceramics”, Journal of Biomaterials Applications 24 (2009) 139-158.

[97] M. Descamps, O. Richart, P. Hardouin, J.C. Hornez, A. Leriche, “Synthesis of macroporous β-tricalcium phosphate with controlled porous architectural”, Ceramics International 34 (2008) 1131-1137.

[98] R. Famery, N. Richard, P. Boch, “Preparation of α- and β-tricalcium phosphate ceramics, with and without magnesium addition”, Ceramics International 20 (1994) 327-336.

[99] K. Sugiyama, M. Tokonami, “Structure and crystal chemistry of a dense polymorph of tricalcium phosphate $Ca_3(PO_4)_2$: A host to accommodate large lithophile elements in the earth’s mantle”, Physics and Chemistry of Minerals 15 (1987), 125-130.

[100] L. Liang, P. Rulis, W.Y. Ching, “Mechanical properties, electronic structure and bonding of α- and β-tricalcium phosphates with surface characterization”, Acta Biomaterialia 6 (2010) 123-132.

[101] B. Dickens, L. W. Schroeder, W. E. Brown, “The crystal structure of pure β-$Ca_3(PO_4)_2$”, Journal of Solid State Chemistry 10 (1974) 232-248.

[102] M. Yashima, A. Sakai, T. Kamiyama, A. Hoshikawa, “Crystal structure analysis of β-tricalcium phosphate $Ca_3(PO_4)_2$ by neutron powder diffraction”, Journal of Solid State Chemistry 175 (2003) 272-277.

[103] K. Lin, J. Chang, J. Lu, W. Wu, Y. Zeng, “Properties of β-$Ca_3(PO_4)_2$ bioceramics prepared using nano-size powders”, Ceramics International 33 (2007) 979-985.

[104] F. Pecqueux, F. Tancret, N. Payraudeau, J.M. Bouler, “Influence of microporosity and macroporosity on the mechanical properties of biphasic calcium phosphate bioceramics: maodeling and experiment”, Journal of the European Ceramic Society 30 (2010) 819-829.

[105] K. de Groot, “Effect of porosity and physiochemical properties on the stability, resorption, and strength of calcium phosphate ceramics”, Annals of the New York Academy of Sciences 523 (1988) 227-233.

[106] A. Bignon, J. Chevalier, G. Fantozzi, “Effect of micro- and macroporosity of bone substitutes on their mechanical properties and cellular response”, Journal of Materials Science: Materials in Medicine 14 (2003) 1089-1097.

[107] L.J. Gibson, M.F. Ashby, “The mechanics of three-dimensional cellular materials”, Proceeding of the Royal Society of London. Series A. Mathematical and Physical Sciences 382 (1982) 43-59.

[108] J.C. Le Huec, T. Schaeverbeke, D. Clement, J. Faber, A. Le Rebeller, “Influence of porosity on the mechanical resistance of hydroxyapatite ceramics under compressive stress”, Biomaterials 16 (1995) 113-118.

[109] A.S. Wegh, J.P. Singh, R.B. Poeppel, “Dependence of ceramic fracture properties on porosity”, Journal of Materials Science 28 (1993) 3589-3593.

[110] I.M. Martinez, P.A. Valasquez, “Synthesis and stability of α-tricalcium phosphate doped with dicalcium silicate in the system $Ca_3(PO_4)_2$-Ca_2SiO_4”, Materials Characterization 61 (2010) 761-767.

[111] X. Yin, L. Calderin, M.J. Stott, M. Sayer, “Density functional study of structural, electronic and vibrational properties of Mg- and Zn-doped tricalcium phosphate biomaterials”, Biomaterials 23 (2002) 4155-4163.

[112] S.S. Banerjee, S. Tarafder, N.M. Davies, A. Bandyopadhyay, S. Bose, “Understanding the influence of MgO and SrO binary doping on the mechanical and biological properties of β-TCP ceramics”, Acta Biomaterialia 6 (2010) 4167-4174.

[113] Z. Seeley, A. Bandyopadhyay, S. Bose, “Tricalcium phosphate based resorbable ceramics: influence of NaF and CaO addition”, Materials Science and Engineering C 28 (2008) 11-17.

[114] X. Yu, S. Cai, Z. Zhang, X. Gouhua, “Bioactive pyrophosphate glass/beta-tricalcium phosphate composite with high mechanical properties”, Materials Science and Engineering C 28 (2008) 1138-1143.

[115] X. Wei, M. Akinc, “Crystal structure analysis of Si- and Zn-codoped tricalcium phosphate by neutron powder diffraction”, Journal of the American Ceramic Society 90 (2007) 2709-2715.

[116] B.S. Chang, C.K. Lee, K.S. Hong, H.J. Youn, H.S. Ryu, S.S. Chung, K.W. Park, “Osteoconduction at porous hydroxyapatite with various pore configurations”, Biomaterials 21 (2000) 1291-1298.

[117] B.D. Cullity, “Elements of X-ray Diffraction”, Second Edition, Addison-Wesley Publishing Company, Reading, MA, USA (1978) 501.

[118] J.E. Hilliard, “Estimating grain size by the intercept method”, Metal Progress Data Sheet (1964) 99-102.

[119] G.F. Kamst, J. Vasseur, C. Bonazzi, J.J. Bimbenet, “A new method for the measurement of the tensile strength of rice grains by using the diametral compression test”, Journal of Food Engineering 40 (1999) 227-232.

[120] J. Jang, S. Kim, “Factors affecting diametral tensile strength of microfilled dental composites”, Polymer Journal 28 (1996) 293-298.

[121] K.A. Gross, L.M. Rodriguez-Lorenzo, “Sintered hydroxyfluorapatites, part I: Sintering ability of precipitated solid solution powders”, Biomaterials 25 (2004) 1375-1384.

[122] M. Descamps, J.C. Hornez, A. Lerich, “Effect of powders stoichiometry on the sintering of β-tricalcium phosphate”, Journal of the European Ceramic Society 27 (2007) 2401-2406.

[123] N. Douard, R. Detsch, R.C. Ghodsina, C. Damia, U. Deisinger, E. Champion, “Processing, Physico-chemical characterisation and in vitro evaluation of silicon containing β-tricalcium phosphate ceramics”, Materials Science and Engineering C 31 (2011) 531-539.

[124] P.E. Wang, T.K. Chaki, “Mechanical Properties of Sintered Calcium Phosphates”, Bioceramics: Materials and Applications / edited by G. Fischman, A. Clare, L. Hench, Ceramic Transactions 48 (1995) 225-234.

[125] H. Qu, M. Wei, “Effect of fluorine content on mechanical properties of sintered hydroxyapatite”, Materials Science and Engineering C 26 (2006) 46-53.

[126] M. Okazaki, H. Tohda., T. Yanagisava, M. Taira, J. Takahashi, “Heterogeneous fluoridated apatites synthesized with a three-step fluoride supply system”, Biomaterials 19 (1998) 919-923.

[127] M. Okazaki, Y. Miake, H. Tohda, T. Yanagisava, T. Matsumoto, J. Takahashi, “Functionally graded fluoridated apatites”, Biomaterials 20 (1999) 1421-1426.

[128] M.V. Regi, J. Pena, I.I. Barba, “Synthesis of β-tricalcium phosphate in layered or powdered forms for biomedical applications”, Solid State Ionics 172 (2004) 445-449.

[129] R.D. Shannon, “Revised effective ionic-radii and systematic studies of interatomic distances in halides and chalcogenides”, Acta Crystallographica Section A 32 (1976) 751-767.

[130] K. Kawabata, T. Yamamoto, A. Kitada, “Substitution mechanism of Zn ions in β-tricalcium phosphate”, Physics B (2010) doi:10.1016/j.physb.2010.12.022.

[131] A. Slosarczyk, C. Paluszkiewicz, M. Gawlicki, Z. Paszkiewicz, “The FTIR spectroscopy and QXRD studies of calcium phosphate based materials produced from the powder precursors with different Ca/P ratios”, Ceramics International 23 (1997) 297-304.

[132] J. Torrent-Burgues, R. Rodriguez-Clemente, “Hydroxyapatite precipitation in a semibatch process”, Crystal Research and Technology 36 (2001) 1075-1082.

[133] S. Kannan, J.M. Ferreira,“Synthesis and thermal stability of hydroxyapatite-beta-tricalcium phosphate composites with cosubstituted sodium, magnesium, and fluorine”, Chemistry of Materials 18 (2006) 198-203.

[134] K.A. Gross, L.M. Rodriguez-Lorenzo, “Sintered hydroxyfluorapatites. Part II: Mechanical properties of solid solutions determined by microindentation”, Biomaterials 25 (2004) 1385–1394.

[135] H. Eslami, M. Solati-Hashjin, M. Tahriri, “The comparison of powder characteristics and physicochemical, mechanical and biological properties between nanostructure ceramics of hydroxyapatite and fluoridated hydroxyapatite”, Materials Science and Engineering C 29 (2009) 1387-1398.

[136] L.J. Jha, M. Best, J.C. Knowles, I. Rehman, J.D. Santos, W. Bonfield, “Preparation and characterization of fluoride substituted apatites”, Journal of Materials Science: Materials in Medicine 8 (1997) 185-191.

[137] H.W. Kim, Y.J. Noh, Y.H. Koh, H.E. Kim, “Enhanced performance of fluorine substituted hydroxyapatite composites for hard tissue engineering”, Journal of Materials Science: Materials in Medicine 14 (2003) 899-904.

[138] M. Azami, S. Jalilifiroozinezhad, M. Mozafari, M. Rabiee, “Synthesis and solubility of calcium fluoride/hydroxy-fluorapatite for dental application”, Ceramics International (2008), doi:10.1016/j.ceramint.2011.02.025.

[139] P. Nongkynrih, S. Troy, S. K. Gupta, P. V. Rao, “Crystal structure of the substituted apatites-deviation from Vegard’s Law”, Journal of Materials Science 23 (1988) 3243-3247.

[140] B. Basar, A. Tezcaner, D. Keskin, Z. Evis, “Improvements in microstructural, mechanical, and biocompatibility properties of nano-sized hydroxyapatites doped with yttrium and fluoride”, Ceramics International 36 (2010) 1633-1643.

[141] Z. Evis, R.H. Doremus, “Effect of YF_3 on hot-pressed hydroxyapatite and monoclinic zirconia composites”, Materials Chemistry and Physics 105 (2007) 76-79.

[142] Z. Evis, F. Ozturk, “Investigation of tensile strength of hydroxyapatite with various porosities by diametral strength test”, Materials Science and Technology 24 (2008) 274-278.

[143] K. T. Chau, X. X. Wei, “A new analytic solution for the diametral point load strength on finite solid circular cylinders”, International Journal of Solids and Structures 38 (2001) 1459-1481.

[144] A. Bigi, E. Foresti, R. Gregorini, A. Ripamonti, N. Roveri, J. S. Shah, “The role of magnesium on the structure of biological apatite”, Calcified Tissue International 50 (1992) 439-444.

[145] V.S. Komlev, S.M. Barinov, F. Rustichelli, “Strength enhancement of porous hydroxyapatite ceramics by polymer impregnation”, Journal of Materials Science Letters 22 (2003) 1215-1217.

[146] S. Best, W. Bonfield, C. Doyle, “In Proceedings of the Second International Symposium on Ceramics in Medicine”, edited by Heimke G., Heidelberg, Germany (1989) 57-64.

[147] A. Slosarczyk, C. Paluszkiewicz, M. Gawlicki, Z. Paszkiewicz, “The FTIR spectroscopy and QXRD studies of calcium phosphate based materials produced from the powder precursors with different Ca/P ratios”, Ceramics International 23 (1997) 297-304.

[148] S. Kannan, J.M.F Ferreira, “Synthesis and thermal stability of hydroxyapatite-beta-tricalcium phosphate composites with cosubstituted sodium, magnesium, and fluorine”, Chemistry of Materials 18 (2006) 198-203.